Phenomenological study of the anisotropic quark matter in the 2-flavor Nambu–Jona–Lasinio model[*]

He-Xia Zhang (https://orcid.org/0000-0001-6871-1579),[1, 2, †] Yu-Xin Xiao,[1]
Jin-Wen Kang,[1] and Ben-Wei Zhang (https://orcid.org/0000-0001-6075-6609)[1, 2, ‡]

[1]*Key Laboratory of Quark & Lepton Physics (MOE) and Institute of Particle Physics,
Central China Normal University, Wuhan 430079, China*
[2]*Guangdong Provincial Key Laboratory of Nuclear Science, Institute of Quantum Matter,
South China Normal University, Guangzhou 510006, China.*

With the two flavor Nambu–Jona–Lasinio (NJL) model, we carried out a phenomenological study on the chiral phase structure, mesonic properties, and transport properties of momentum-space anisotropic quark matter. To calculate the transport coefficients we utilized the kinetic theory in the relaxation time approximation, where the momentum anisotropy is embedded in the estimation of both the distribution function and relaxation time. It was shown that an increase in the anisotropy parameter ξ may result in a catalysis of chiral symmetry breaking. The critical endpoint (CEP) is shifted to lower temperatures and larger quark chemical potentials as ξ increases, and the impact of momentum anisotropy on the CEP temperature is almost the same as that on the quark chemical potential of the CEP. The meson masses and the associated decay widths also exhibit a significant ξ dependence. It was observed that the temperature behavior of the scaled shear viscosity η/T^3 and scaled electrical conductivity $\sigma_{\rm el}/T$ exhibited a similar dip structure, with the minima of both η/T^3 and $\sigma_{\rm el}/T$ shifting toward higher temperatures with increasing ξ. Furthermore, we demonstrated that the Seebeck coefficient S decreases when the temperature rises and its sign is positive, indicating that the dominant carriers for converting the temperature gradient to the electric field are up-quarks. The Seebeck coefficient S is significantly enhanced with a large ξ for a temperature below the critical temperature.

Keywords: Heavy-ion collision, Momentum anisotropy, NJL model, Chiral phase transiton, Transport coefficient, Quark matter

I. INTRODUCTION

The properties of strongly interacting matter described by the quantum chromodynamics (QCD) in extreme conditions of temperature T and density have aroused a plethora of experimental studies in the last thirty years [1, 2]. The experiment studies performed at the Relativistic Heavy Ion Collider (RHIC) in BNL and the Large Hadron Collider (LHC) in CERN have revealed that a new deconfined state of matter, the quark-gluon plasma (QGP), can be created at high temperature. Further, the non-central heavy-ion collisions produce the strongest magnetic fields and orbital angular momenta, which can induce a number of novel phenomena [3–5]. The lattice QCD calculation, which is a powerful gauge invariant approach to investigate the non-perturbative properties, has also confirmed that the phase transition is a smooth and continuous crossover for vanishing chemical potential [6, 7]. Owing to the so-called fermion sign problem [8], lattice QCD simulation is limited to low finite density [9, 10], even though several calculation techniques, such as the Taylor expansion [11, 12], analytic continuations from imaginary to real chemical potential [13, 14], and multi-parameter reweighting method [15], have been proposed to address this problem and improve the validity at high chem-

ical potential. More detailed reviews of lattice calculation can be found in Refs. [16, 17]. Alternatively, one also can rely on effective models, the Dyson–Schwinger equation approach [18, 19] and the functional renormalization group approach [20, 21], to study the chiral aspect of QCD for finite baryon chemical potential $\mu_{\rm B}$. Currently, there are various QCD inspired effective models, such as the Nambu–Jona–Lasinio (NJL) model [22, 23], Polyakov-loop enhanced NJL (PNJL) model [24, 25], Quark-Meson (QM) model [26, 27], and Polyakov QM (PQM) model [28, 29], which not only can successfully describe the spontaneous chiral symmetry breaking and restoration of QCD but also have been applied to explore the QCD phase structure and internal properties of the meson at arbitrary T and $\mu_{\rm B}$. These model calculations have predicted that at high chemical potential, the phase transition is a first-order phase transition, and with decreasing $\mu_{\rm B}$, the first-order phase transition has to end at a critical end point (CEP) and change into a crossover. At this CEP the phase transition is of second order. However, owing to various approximations adopted in the model calculations, there is no agreement on the existence and location of the CEP in the phase diagram. Furthermore, the rotation effects [30, 31], magnetic field effects [32–35], finite-volume effects [36–40], non-extensive effects [41, 42], external electric fields [43–45], and chiral chemical potential effects [46–49] have also been considered in the effective models to provide a better insight into the phase transition of the realistic QCD plasma.

Apart from the QCD phase structure information, the transport coefficients, characterizing the non-equilibrium dynamical evolution of QCD matter in heavy-ion collisions [50–52], have also attracted significant attention. The shear viscosity η, which quantifies the rate of momentum transfer in a

fluid with inhomogeneous flow velocity, has been successfully used in the viscous relativistic hydrodynamic description of the QGP bulk dynamics. The small shear viscosity to entropy density ratio η/s can be extracted from the elliptic flow data [53]. In the literature, there are various frameworks for estimating the η of strongly interacting matter, e.g., the kinetic theory within the relaxation time approximation (RTA), QCD effective models [54–58], the quasiparticle model (QPM) [59, 60], and the lattice QCD simulation [61]. The electrical conductivity $\sigma_{\rm el}$, as the response of a medium to an applied electric field, has also attracted attention in high energy physics. The presence of $\sigma_{\rm el}$ not only can affect the duration and strength of magnetic fields [62], but also is directly proportional to the emissivity and production of soft photons [63, 64]. The thermal behavior of $\sigma_{\rm el}$ has been estimated using different approaches, such as the microscopic transport models [65–67], lattice gauge theory simulation [68, 69], hadron resonance gas model [70, 71], quasiparticle models [72, 73], effective models [54, 74], string percolation model [75], and holographic method [76]. Recently, studies of electrical conductivity in QGP in the presence of magnetic fields have also been performed [77–79]. Another less concerned but interesting coefficient is the Seebeck coefficient (also called thermopower). When a spatial gradient of temperature exists in a conducting medium, a corresponding electric field can arise and vice versa, which is the Seebeck effect. When the electric current induced by an electric field can compensate with the current owing to the temperature gradient, the thermal diffusion ends. Accordingly, the efficiency of converting the temperature gradient to an electric field in the open circuit condition is quantified by the Seebeck coefficient S. In past years, the Seebeck effect has been extensively investigated in condensed matter physics. Very recently, the exploration has been extended to the hot QCD matter. For example, the Seebeck coefficient with and without magnetic fields has been studied in both the hadronic matter [80, 81] and QGP [82, 83]. In Ref. [84], the Seebeck coefficient has also been estimated based on the NJL model, where the spatial gradient of the quark chemical potential is considered in addition to the presence of a temperature gradient.

In the initial stages of a HIC, the pressure gradient of the created fireball along the beam direction (denoted as longitudinal z direction) is significantly lower than that along the transverse direction. After the rapid expansion of the medium along the beam direction, the system becomes much colder in the beam direction than the transverse direction, which causes the QGP to possess a local momentum anisotropy, and this anisotropy can survive during the entire evolution of the medium [85]. In addition, the presence of a strong magnetic field can also induce a local anisotropy in the momentum space. Inspired by the presence of momentum-space anisotropy in HICs, the primary objective of the present work is to study phenomenologically its effect on the chiral phase structure, mesonic properties, and transport coefficients in the SU(2) NJL model. To incorporate the momentum anisotropy into numerical calculations, we follow the anisotropic distribution function parametrization method proposed by Romatschke and Strickland [86], $f^{\rm aniso}(\mathbf{p}) \rightarrow$

$f^{\rm iso}(\sqrt{\mathbf{p}^2 + \xi(\mathbf{p} \cdot \mathbf{n})^2})$. Here, the isotropic momentum-space distribution function of particle ($f^{\rm iso}$) is deformed by rescaling one preferred direction in the momentum space with the unit vector $\mathbf{n}$ and introducing the directional dependent parameter ξ, which is used to quantify the degree of momentum-space anisotropy. This method has been extensively employed to study phenomenologically the impacts of momentum anisotropy on various observables, such as photon production [87, 88], parton self-energy [89, 90], heavy-quark potential [91], and various transport coefficients [92–94]. The relativistic anisotropic hydrodynamics (aHydro) models can provide a more accurate description of non-equilibrium dynamics compared to other hydrodynamical models [95]. As in most previous studies, the focus of the present work is on the weakly anisotropic medium (very close to the equilibrium) for which $|\xi| \ll 1$ and the distribution function can be expanded up to linear order in ξ. We found that even for small values of anisotropy, the effective quark mass and meson masses change significantly compared to the equilibrium result. Unlike most momentum anisotropy studies of transport coefficients in QGP, in which the effect of momentum anisotropy is not considered in the different particle interaction channels, in the present work, we incorporated the momentum anisotropy to the estimation of the relaxation time to better study the impact of ξ on transport properties of quark matter near the phase transition temperature region.

This paper is organized as follows: Sect. II provides a brief review of the basic formalism of the 2-flavor NJL model. In Sect. III and Sect. IV, we present a brief derivation of the expressions associated with the constituent quark mass and meson mass spectrum in both an isotropic and anisotropic medium. Section V includes the detailed procedure for obtaining the formulae of momentum-anisotropy-dependent transport coefficients. In Sect. VI, we present the estimation of the relaxation time for (anti-)quarks. The numerical results for various observables are phenomenologically analyzed in Sect. VII. In Sect. VIII, the present work is summarized with an outlook. The formulae for the squared matrix elements in different quark-(anti-)quark elastic scattering processes are presented in the Appendix.

II. THEORETICAL FRAME

In this work, we start from the standard two-flavor NJL model, which is a purely fermionic theory owing to the absence of all gluonic degrees of freedom. Accordingly, the lagrangian is given as [22]

$$\mathcal{L} = \bar{\psi}(i\partial - \hat{m}_0)\psi + G[(\bar{\psi}\psi)^2 + (\bar{\psi}i\gamma_5\hat{\tau}\psi)^2], \quad (1)$$

where $\psi(\bar{\psi})$ stands for the quark (antiquark) field with two-flavors (u, d) $N_{\rm f} = 2$ and three colors $N_{\rm c} = 3$. $\hat{m}_0$ denotes the diagonal matrix of the current quark mass of up and down-quarks, and we take $m_0 = m_u^0 = m_d^0$ to ensure isospin symmetry of the NJL lagrangian. G is the effective coupling strength of four-point fermion interaction in the scalar and pseudoscalar channels. $\hat{\tau}$ is the vector of the Pauli matrix in the isospin space.

In the NJL model, under the mean field (or Hartree) approximation [22, 23], the quark self-energy is momentum-independent and can be identified as the constituent quark mass m_q, which acts as order parameter for characterizing the chiral phase transition. For an off-equilibrium system, the evolution of the space–time dependence of the constituent quark mass in the real time formalism can be obtained by solving the gap equation [96]

$$m_q = m_0 - 2Gi\mathrm{Tr}iS^<(x,x), \qquad (2)$$

where $S^<(x,y) = i\langle\bar{\psi}(y)\psi(x)\rangle$ with $x = (t, \mathbf{x})$ is the real time Green function in the coordinate space [97, 98], $\langle\dots\rangle$ denotes the thermal average, and the trace runs over spin, color, and flavor degrees of freedom. Transforming Eq. (2) to the phase space with the help of Winger transformation and introducing the quasiparticle approximation (see Ref. [99] for details), the gap equation can be further written as [96, 98–100]

$$m_q = m_0 + 4N_\mathrm{f}N_\mathrm{c}\int\frac{d^3\mathbf{p}}{(2\pi)^3}\frac{m_\mathrm{q}}{E_\mathbf{p}}\left(1 - f_q(x,\mathbf{p}) - \bar{f}_{\bar{q}}(x,\mathbf{p})\right), \qquad (3)$$

where $E_\mathbf{p} = \sqrt{\mathbf{p}^2 + m_q^2(x)}$ is the quasi-quark energy. As the NJL model is a non-renormalizable model owing to the point-like four fermion interaction in the lagrangian, an ultraviolet cutoff Λ is used to regularize the divergent integral. In the non-equilibrium case, the space–time evolution of the one-particle distribution function $f(x,\mathbf{p})$ in Eq. (3) is described by the Boltzmann–Vlasov transport equation from the NJL model in the Hartree level [100–102]. By solving the Vlasov equation together with the gap equation concurrently, the constituent quark mass affecting the space–time dependence of $f(x,\mathbf{p})$ can be determined self-consistently.

To better understand the meson dynamics in HICs, it is useful to study the structure of the meson propagation in the medium. In the framework of the NJL model, mesons are bound states of quarks and antiquarks (collective modes), and the meson propagator can be constructed by calculating the quark–antiquark effective scattering amplitude within the random phase approximation (RPA) [23, 96, 98]. Following Refs. [96, 98], the explicit form for the pion (π) and the sigma meson (σ) propagators in the RPA reads as

$$D_M(x, k_0, \mathbf{k}) = \frac{2iG}{1 - 2G\Pi_M(x, k_0, \mathbf{k})}. \qquad (4)$$

All information of a meson is contained in the irreducible one-loop pseudoscalar or scalar polarization function Π_M, where the subscript M corresponds to pseudoscalar (π) or scalar (σ) mesons. The space–time dependence of the polarization function in a non-equilibrium system is given as [96, 98]

$$\Pi_M = N_\mathrm{c}N_\mathrm{f}\int\frac{d^3\mathbf{p}}{4\pi^3}\frac{1}{E_\mathbf{p}}[1 - f_q(x,\mathbf{p}) - f_{\bar{q}}(x,\mathbf{p})]$$
$$\times\left\{1 - \frac{(k_0^2 - \mathbf{k}^2 - \nu_M^2)}{2E_{\mathbf{p-k}}}\left[\frac{E_\mathbf{p} + E_{\mathbf{p-k}}}{k_0^2 - (E_\mathbf{p} + E_{\mathbf{p-k}})^2}\right.\right.$$
$$\left.\left. - \frac{E_\mathbf{p} - E_{\mathbf{p-k}}}{k_0^2 - (E_\mathbf{p} - E_{\mathbf{p-k}})^2}\right]\right\}. \qquad (5)$$

Here, ν_M denotes the real value of the bound meson energy, and $\nu_M = 0\ (2m_q)$ for the π (σ) meson.

III. CONSTITUENT QUARK AND MESON IN AN ISOTROPIC QUARK MATTER

In an expanding system (e.g., the dynamical process of heavy-ion collisions), the space–time dependence in the phase–space distribution function is hidden in the space–time dependence of temperature and chemical potential. However, for a uniform temperature and chemical potential, i.e., for a system in global equilibrium, the distribution function is well defined and independent of space–time. Therefore, in the equilibrium (isotropic) state, to investigate the chiral phase transition and mesonic properties within the NJL model, one can employ the imaginary-time formalism. Actually, the results in Ref. [96] have indicated that the real-time calculation of the closed time-path Green's function reproduces exactly the finite temperature result of the NJL model obtained from the Matsubara's temperature Green's function in the thermo-dynamical equilibrium limit. In the following, we will briefly present the procedure for the derivation of the polarization function in the imaginary time formalism. In an equilibrium system, m_q, which is temperature- and quark chemical potential-dependent, can be directly calculated from the self-consistent gap equation in momentum space [22, 23]:

$$m_q = m_0 + 4GN_\mathrm{f}N_\mathrm{c}\int\frac{d^3\mathbf{p}}{(2\pi)^3}\frac{m_q}{E_\mathbf{p}}\left(1 - f_q^0(\mathbf{p}) - \bar{f}_{\bar{q}}^0(\mathbf{p})\right). \qquad (6)$$

We can see that by taking the thermal equilibrium distribution functions (Fermi–Dirac distributions), Eq. (3) has the same form as Eq. (6). The equilibrium distribution function of (anti-)quark $f_{q(\bar{q})}^0$ is given by

$$f_{q(\bar{q})}^0(\mathbf{p}) = [\exp[(E_\mathbf{p} - \mu_{q(\bar{q})})\beta] + 1]^{-1}, \qquad (7)$$

where $\beta = 1/T$ is the inverse temperature of the system, and a uniform quark chemical potential $\mu \equiv \mu_{u,d} \equiv -\mu_{\bar{u},\bar{d}}$ is assumed. It is noted that the ultraviolet divergence is not presented in the integrand containing Fermi–Dirac distribution functions, so the momentum integral do not need to be regularized for finite temperatures. In the equilibrium, the meson propagator is given as [57]

$$D_M(k_0, \mathbf{k}) = \frac{2iG}{1 - 2G\Pi_M(k_0, \mathbf{k})}, \qquad (8)$$

where Π_M at an arbitrary temperature and quark chemical potential is given by [103, 104]

$$\Pi_M(k_0, \mathbf{k}) = -\frac{N_\mathrm{c}N_\mathrm{f}}{8\pi^2}[((m_q \mp m_q)^2 - k_0^2 + \mathbf{k}^2)$$
$$\times B_0(k_0, \mathbf{k}, \mu, T, m_q) + 2A(\mu, T, m_q)]. \qquad (9)$$

The minus (plus) sign refers to pseudoscalar (scalar) mesons. The function A, which relates to the one-fermion-line integral, in the imaginary time formalism for finite temperatures

and quark chemical potentials is given as [103]

$$A = \frac{16\pi^2}{\beta} \sum_n \exp(i\omega_n y) \int \frac{d^3\mathbf{p}}{(2\pi)^3} \frac{1}{(i\omega_n + \mu)^2 - E_{\mathbf{p}}^2},$$
(10)

where $\omega_n = (2n+1)\pi/\beta$ are the fermionic Matsubara frequencies and the sum of n runs over all positive and negative integer values. It is to be understood that the limit $y \to 0$ is to be taken after the Matsubara summation. The function B_0 in Eq. (9) relates to the two-fermion-line integral. At finite μ and T, B_0 is defined as [103]

$$\begin{aligned} &B_0(i\nu_l, \mathbf{k}, \mu, T, m_q) \\ &= \frac{16\pi^2}{\beta} \sum_n \exp(i\omega_n y) \int_{|\vec{p}|<\Lambda} \frac{d^3\mathbf{p}}{(2\pi)^3} \frac{1}{((i\omega_n + \mu)^2 - E^2)} \\ &\times \frac{1}{((i\omega_n - i\nu_l + \mu)^2 - E'^2)}, \end{aligned}$$
(11)

where we have abbreviated $E' = E_{\mathbf{p}-\mathbf{k}} = \sqrt{(\mathbf{p}-\mathbf{k})^2 + m_q^2}$ and $E = E_{\mathbf{p}}$ for convenience, and after the Matsubara summation on n is carried out, the complex frequencies $i\nu_l$ are analytically continued to their values on the real plane, i.e., $i\nu_l \to k_0 - i\epsilon$ ($\epsilon > 0$) with k_0 being the zero component of the associated four-momentum. The full calculations of functions A and B_0 at arbitrary values of temperature and chemical potential can be found in Ref. [105]. After evaluating the Matsubara summation by contour integration in the usual fashion [106], Eq. (10) is given as

$$A = 8\pi^2 \int \frac{d^3\mathbf{p}}{(2\pi)^3 E_{\mathbf{p}}} (f_q^0 + f_{\bar{q}}^0 - 1),$$
(12)

where the Fermi–Dirac distribution function is introduced. Similar to the treatment of function A, after Matsubara summation over n and the Matsubara frequencies $i\nu_l$ are analytically continued to real values, Eq. (11) can be rewritten in the following form:

$$\begin{aligned} &B_0(k_0, \mathbf{k}, \mu, T, m_q) \\ &= 16\pi^2 \int \frac{d^3\mathbf{p}}{(2\pi)^3} \frac{f_q^0(p) + f_{\bar{q}}^0(p) - 1}{2E} \\ &\times \left[\frac{1}{(E + i\nu_l)^2 - (E')^2} + \frac{1}{(E - i\nu_l) - (E')^2} \right]. \end{aligned}$$
(13)

Inserting Eqs. (12) and (13) to Eq. (9), we finally can obtain the expression for Π_M in the equilibrium state, which is formally the same as Eq. (5), except that the distribution functions are ideal Fermi–Dirac distribution functions rather than space–time dependent distribution functions.

IV. CONSTITUENT QUARK AND MESON IN A WEAKLY ANISOTROPIC MEDIUM

As mentioned in the introduction, the consideration of momentum anisotropy induced by rapid expansion of the hot QCD medium for existing phenomenological applications is mostly achieved by parameterizing the associated isotropic distribution functions. To proceed with the numerical calculation, a specific form of anisotropic (non-equilibrium) momentum distribution function is required. In this work, we utilized the Romatschke–Strickland (RS) form [86] in which the system exhibits a spheroidal momentum anisotropy, and the anisotropic distribution was obtained from an arbitrary isotropic distribution function by removing the particle with a momentum component along the direction of anisotropy, $f^{\text{aniso}}(\mathbf{p}) = f^{\text{iso}}(\sqrt{\mathbf{p}^2 + \xi(\mathbf{p}\cdot\mathbf{n})^2})$, where $\mathbf{n}$ and ξ are, respectively, the anisotropy direction and anisotropy parameter. As in previous studies [107], we shall restrict ourselves here to a plasma close to local thermal equilibrium, i.e., close to isotropy in the momentum space. Accordingly, the explicit form of anisotropic momentum distribution function in the local rest frame can be written as

$$f^{\text{aniso}}(\mathbf{p}) = \frac{1}{\exp[(\sqrt{\mathbf{p}^2 + \xi(\mathbf{p}\cdot\mathbf{n})^2 + m_q^2} - \mu'_{q(\bar{q})})/T'] + 1},$$
(14)

It is worth noting that for the anisotropic (non-equilibrium) matter, the T' and μ' appearing in Eq. (14) lose the usual meaning of T and μ in the equilibrium system and may have dimensionful scales related to the mean particle momentum [108]. If we assume the system to be very close to the equilibrium (in the small anisotropy limit), then the parameters T' and μ' still could be taken to be the usual T and μ, respectively, as performed in previous studies [92–94, 107]. The anisotropy parameter ξ is defined as $\xi = \langle p_\perp^2 \rangle / (2\langle p_\parallel^2 \rangle) - 1$, where $p_\perp = |\mathbf{p} - (\mathbf{p}\cdot\mathbf{n})\cdot\mathbf{n}|$ and $p_\parallel = \mathbf{p}\cdot\mathbf{n}$ are the momentum components of particles perpendicular and parallel to $\mathbf{n}$, respectively. As the precise time evolution of ξ is still an open question, we assume that the anisotropy parameter ξ in a local anisotropic system is constant and independent of time, where $-1 < \xi < 0$ corresponds to a contraction of momentum distribution along the direction of anisotropy and $\xi > 0$ corresponds to a stretching of momentum distribution along the direction of anisotropy. In Eq. (14), the three-velocity of partons and anisotropy unit vector are selected as

$$\mathbf{n} = (\sin\chi, 0, \cos\chi),$$
(15)

$$\mathbf{p} = p(\sin\theta\cos\phi, \sin\theta\sin\phi, \cos\theta),$$
(16)

where χ is the angle between $\mathbf{p}$ and $\mathbf{n}$, and $p \equiv |\mathbf{p}|$ throughout the computations. With this choice, the spheroidally anisotropic term, $\xi(\mathbf{n}\cdot\mathbf{p})^2$ in Eq. (14) can be written as $\xi(\mathbf{n}\cdot\mathbf{p})^2 = \xi p^2(\sin\chi\cos\phi\sin\theta + \cos\chi\cos\theta)^2 = \xi c(\theta, \phi, \chi)$. We further assume that $\mathbf{n}$ points along the beam (z) axis, i.e., $\mathbf{n} = (0, 0, 1)$. It is essential to note that we shall restrict ourselves here to a plasma close to the equilibrium state and have small anisotropy around the equilibrium state. Therefore, in the weak anisotropy limit ($|\xi| \ll 1$), one can expand Eq. (14) around the isotropic limit and retain only the leading order in ξ. Accordingly, the anisotropic momentum distribution function in the local rest frame can be further written as [107]

$$f^{\text{aniso}}(\mathbf{p}) = f^0 - \frac{\xi(\mathbf{n}\cdot\mathbf{p})^2}{2ET} f^0(1 - f^0),$$
(17)

where the second term is the anisotropic correction to the equilibrium distribution, which is also related to the leading-order viscous correction to the equilibrium distribution in viscous hydrodynamics. For a fluid expanding one-dimensionally along the direction $\mathbf{n}$ in the Navier–Stokes limit, the explicit relation is given as [109, 110]

$$\xi = \frac{10}{T\tau}\frac{\eta}{s}, \qquad (18)$$

which indicates that the non-zero shear viscosity (finite momentum relaxation rate) in an expanding system can also explicitly lead to the presence of momentum-space anisotropy. At the RHIC energy with the critical temperature $T_c \approx 160$ MeV, $\tau \approx 6$ fm/c and $\eta/s = 1/4\pi$, we can obtain $\xi \approx 0.3$. In principle, for the non-equilibrium dynamics of the chiral phase transition, a self-consistent numerical study must be performed by solving the Boltzmann–Vlasov transport equation together with gap equation in terms of the space–time dependent quark distribution as mentioned in Sect. II. However, because the non-equilibrium distribution function in the local rest frame of weakly anisotropic systems has a specific form and the temperature and chemical potential appearing in Eq. (17) are still considered as free parameters, the space–time evolution is not addressed. Therefore, in the non-equilibrium states possessing small momentum space anisotropy, just by solving the gap equation with anisotropic momentum distribution, i.e., Eq. (17), it is possible for us to investigate phenomenologically the impact of momentum anisotropy on the temperature and quark potential dependence of the constituent quark mass. Accordingly, the gap equation, i.e., Eq. (2) or Eq. (6), is modified as

$$0 = \left[2N_c N_f G \int_0^\infty \frac{p^2 dp}{\pi^2}\frac{m_q}{E}\left(-f_q^0 - f_{\bar{q}}^0 + 1 + \frac{p^2\xi F_p}{6ET}\right)\right] + m_0 - m_q. \qquad (19)$$

Here, we have abbreviated $F_p = f_q^0(1-f_q^0) + f_{\bar{q}}^0(1-f_{\bar{q}}^0)$ for convenience. The momentum anisotropy is also embedded in the study of mesonic properties by substituting the anisotropic momentum distribution in the A function part of Eq. (5), thus obtaining

$$A = 4\int \frac{p^2 dp}{E}\left[f_q^0 + f_{\bar{q}}^0 - 1 - \frac{\xi p^2 F_p}{6ET}\right]. \qquad (20)$$

In the $\xi \to 0$ limit, the above equation reduces to Eq. (12). Similar to the treatment of function A, the weak momentum anisotropy effects can enter the B_0 function (as given in Eq. (5) or Eq. (13)) by using the anisotropic momentum distribution. Without loss of generality, we selected the coordinate system in such a way that $\mathbf{k}$ is parallel to the z-axis, i.e.,

$$\mathbf{k} = (0,0,k), \quad |\mathbf{k}| \equiv k. \qquad (21)$$

We first discuss a simple case, i.e., $\mathbf{k} = \mathbf{0}$, $k_0 \neq 0$. The computation of function B_0 in a weakly anisotropic medium

is trivial, viz,

$$B_0 s = 8\pi^2 \int \frac{d^3\mathbf{p}}{(2\pi)^3 E}(f_q^{\text{aniso}}(\mathbf{p}) + f_{\bar{q}}^{\text{aniso}}(\mathbf{p}) - 1)$$
$$\times \left(\frac{1}{k_0^2 - 2Ek_0 + i\epsilon\,\text{sgn}(k_0)} + \frac{1}{k_0^2 + 2Ek_0 - i\epsilon\,\text{sgn}(k_0)}\right). \qquad (22)$$

In the integrand of the above equation, there are two poles at $E = E_0 = \pm k_0/2$ if $m \leq E_0$. Applying the Cauchy formula

$$\lim_{\epsilon \to 0}\frac{1}{x - i\epsilon} = \mathcal{P}\frac{1}{x} + i\pi\delta(x), \qquad (23)$$

where $\mathcal{P}$ denotes the Cauchy principal value. The function B_0 can finally be rewritten as

$$B_0 = 8\mathcal{P}\int \frac{p^2 dp}{E(k_0^2 - 4E^2)}[f_q^0(\mathbf{p}) + f_{\bar{q}}^0(\mathbf{p}) - 1 - \frac{\xi p^2}{6ET}F_p]$$
$$-i\pi\frac{2}{k_0}\left[\left(f_q^0(z_0) + f_{\bar{q}}^0(z_0) - 1 - \frac{\xi z_0^2}{3k_0 T}F_{z_0}\right)\right.$$
$$\left.\times \sqrt{(\frac{k_0}{2})^2 - m_q^2}\Theta(\frac{k_0^2}{4} - m_q^2)\right]. \qquad (24)$$

Here, $z_0 = \sqrt{(\frac{k_0}{2})^2 - m_q^2}$, and Θ is the step function to ensure that the imaginary part appears only for $k_0/2 > m_q$. Next, in the case of $k > 0$, $k_0 \neq 0$, the expression for function B_0 is slightly complicated and can be written as

$$B_0 = \frac{1}{k}\int_0^\infty \frac{pdp}{E}(f_q^{\text{aniso}}(\mathbf{p}) + f_{\bar{q}}^{\text{aniso}}(\mathbf{p}) - 1))$$
$$\times \int_{-1}^1 dx\left(\frac{1}{x + (k_0^2 + 2k_0 E - k^2)/2pk - i\epsilon\,\text{sgn}(k_0)}\right.$$
$$\left.+ \frac{1}{x + (k_0^2 - 2k_0 E - k^2)/2pk + i\epsilon\,\text{sgn}(k_0)}\right)$$
$$= B_0^{\text{an}} + B_0^{\text{iso}}, \qquad (25)$$

with the abbreviation $x = \cos\theta$. The isotropic part B_0^{iso} reads as

$$B_0^{\text{iso}} = \frac{1}{k}\int_0^\infty \frac{pdp}{E}\left(f_q^0 + f_{\bar{q}}^0 - 1\right)$$
$$\times \left[\log\left|\frac{(k_0^2 - k^2 + 2pk)^2 - (2k_0 E)^2}{(k_0^2 + k^2 - 2pk)^2 - (2k_0 E)^2}\right|\right.$$
$$+ i\pi(\Theta(2pk - |k_0^2 + 2k_0 E - k^2|)$$
$$\left.- \Theta(2pk - |k_0^2 - 2k_0 E - k^2|))\right]. \qquad (26)$$

The anisotropic part B_0^{an} reads as

$$B_0^{\text{aniso}} = -\frac{1}{k}\int_0^\infty \frac{pdp}{E}\frac{\xi p^2 F_p}{2ET}\left[\left(-\frac{(k_0^2-k^2+2k_0E)}{pk}+\left(\frac{k_0^2-k^2+2k_0E}{2pk}\right)^2\log\left|\frac{k_0^2+2k_0E-k^2+2pk}{k_0^2+2k_0E-k^2-2pk}\right|\right.\right.$$
$$-\frac{(k_0^2-k^2-2k_0E)}{pk}+\left(\frac{k_0^2-k^2-2k_0E}{2pk}\right)^2\log\left|\frac{k_0^2-2k_0E-k^2+2pk}{k_0^2-2k_0E-k^2-2pk}\right|\right)$$
$$\left.+i\pi\left(\frac{k_0^2+2k_0E-k^2}{2pk}\Theta(2pk-|k_0^2+2k_0E-k^2|)-\frac{k_0^2-2k_0E-k^2}{2pk}\Theta(2pk-|k_0^2-2k_0E-k^2|)\right)\right]. \quad (27)$$

When $k_0 = 0$, the imaginary part of Eq. (25) vanishes. Therefore, the real and imaginary parts of meson polarization functions for different cases in a weakly anisotropic medium are given by

$$\text{Re}\Pi_M(k_0,0) = N_{\text{f}}N_{\text{c}}\mathcal{P}\int_0^\infty \frac{dpp^2}{\pi^2 E}\left[1-f_q^0(\mathbf{p})-f_{\bar{q}}^0(\mathbf{p})+\frac{\xi p^2}{6ET}F_p\right]\frac{E^2-\nu_M^2/4}{E^2-(k_0/2)^2}, \quad (28)$$

$$\text{Im}\Pi_M(k_0,0) = \frac{N_{\text{c}}N_{\text{f}}}{8\pi k_0}\sqrt{k_0^2-4m_q^2}(k_0^2-\nu_M^2)\left[1-f_q^0(z_0)-f_{\bar{q}}^0(z_0)+\frac{z_0^2\xi}{3k_0T}F_{z_0}\right]\Theta(k_0^2-4m_q^2), \quad (29)$$

$$\text{Re}\Pi_M(0,k) = \frac{N_{\text{c}}N_{\text{f}}}{\pi^2}\int_0^\infty\frac{dpp^2}{E}(1+\frac{k^2+\nu_M^2}{4pk}\ln\left|\frac{k-2p}{k+2p}\right|)\left(1-f_q^0(\mathbf{p})-f_{\bar{q}}^0(\mathbf{p})\right)$$
$$+\frac{N_{\text{c}}N_f}{\pi^2}\int_0^\infty\frac{\xi p^2 dp}{E^2 T}F_p\left[\frac{p^2}{6}+\frac{k^2+\nu_M^2}{4}\left(1+\frac{k^2}{4pk}\ln\left|\frac{k-2p}{k+2p}\right|\right)\right]. \quad (30)$$

Similar to the treatment in Eq. (6), the vacuum divergence in Eqs. (28)-(30) also need to be regularized. When the effect of momentum anisotropy is turned off ($\xi = 0$), Eqs. (28)–(30) are reduced to the results of Ref. [57] in thermal equilibrium. Once the propagators of mesons are given, their masses can be determined by the pole in Eq. (8) at zero three-momentum, i.e.,

$$1-2G\text{Re}\Pi_M(m_{\pi,\sigma},0) = 0. \quad (31)$$

The solution is a real value for $m_{\pi,\sigma} < 2m_q$, and a meson is stable. However, for $m_{\pi,\sigma} > 2m_q$, a meson dissociates to its constituents and becomes a resonant state. Accordingly, the polarization function is a complex function and Π_M has an imaginary part that is related to the decay width of the resonance as $\Gamma_M = \text{Im}\Pi_M(m_{\pi,\sigma},0)/m_{\pi,\sigma}$.

V. TRANSPORT COEFFICIENTS IN AN ANISOTROPIC QUARK MATTER

In this section, we study the effects due to the local anisotropy of the plasma in the momentum space on the transport coefficients (shear viscosity, electrical conductivity, and Seebeck coefficient). The calculation is performed in the kinetic theory that is widely used to describe the evolution of the non-equilibrium many-body system in the dilute limit. Assuming that the system has a slight deviation from the equilibrium, the relaxation time approximation (RTA) can be reasonably employed. The momentum anisotropy is encoded in the phase-space distribution function, which evolves according to the relativistic Boltzmann equation. We provide the following procedures for deriving the ξ-dependent transport coefficients.

A. Shear viscosity

The propagation of a single quasiparticle with temperature- and chemical potential-dependent mass in an anisotropic medium is described by the relativistic Boltzmann–Vlasov equation [101]

$$\left[p^\mu\partial_\mu + \frac{1}{2}\partial^\mu m_a^2\partial_\mu^{(p)}\right]f_a(x,\mathbf{p}) = C[f_a(x,\mathbf{p})], \quad (32)$$

where $\frac{1}{2}\partial^\mu m_a^2$ acts as the force term attributed to the residual mean field interaction. The right-hand side of Eq. (32) is the collision term. Considering that the system has a small departure from the equilibrium due to an external perturbation, the collision term within the RTA can be given as

$$C[f] \simeq -\frac{p^\mu u_\mu[f_a(x,\mathbf{p})-f_a^0(x,\mathbf{p})]}{\tau_a} = -\frac{p^\mu u_\mu\delta f_a}{\tau_a}, \quad (33)$$

in which τ_a denotes the relaxation time for particle species a and can quantify how fast the system reaches the equilibrium again. Near equilibrium, the distribution function can be expanded about a local equilibrium distribution function for the

quarks as

$$f_a = f_a^0(x, \mathbf{p}) + \delta f_a, \qquad (34)$$

with $f_a^0(x, \mathbf{p}) = [\exp((u_\nu(x)p^\nu - \mu_a(x))\beta(x)) + 1]^{-1}$, where $p^\nu \equiv (E_a, \mathbf{p})$ is the particle four-momentum, and $u^\nu = \gamma_\nu(1, \mathbf{u})$ is the fluid four-velocity with $\gamma_\nu = (1 - \mathbf{u}^2)^{1/2}$. δf_a in Eq. (33) is the deviation of the distribution function from the local equilibrium due to the external disturbance, which up to first-order in the gradient expansion can be read as

$$\delta f_a = -\frac{\tau_a}{p^\mu u_\mu}\left[p^\mu \partial_\mu f_a^0 + m_a \frac{dm_a}{dT}(\partial^\mu T)\partial_\mu^{(p)} f_a^0\right], \quad (35)$$

where the four-derivative can be decomposed into $\partial_\mu \equiv \partial/\partial^\mu \equiv u_\mu D + \nabla_\mu$, and $D \equiv u^\mu \partial_\mu$ and $\nabla_\nu \equiv \Delta^{\mu\nu}\partial_\nu$ denote the time derivative and spatial gradient operator in the local rest frame, respectively. $g^{\mu\nu} = diag(1, -1, -1, -1)$ is the metric tensor, and $\Delta^{\mu\nu} = g^{\mu\nu} - u^\mu u^\nu$ is the projection operator orthogonal to u^μ. In the presence of weak momentum anisotropy, the associated covariant version of the weakly anisotropic function f_a^{an} for particle species a can be written as

$$f_a^{\text{aniso}}(x, \mathbf{p}) = \frac{1}{\exp[(\sqrt{(p_\nu u^\nu)^2 + \xi(p_\nu V^\nu)^2} - \mu_a)\beta] + 1}, \qquad (36)$$

$$\approx f_a^0 - \frac{\xi(p^\nu V_\nu)^2}{2Tp^\nu u_\nu}f_a^0(1 - f_a^0), \qquad (37)$$

where $V^\nu = (0, \mathbf{n})$ is defined as the anisotropy vector. Employing Eq. (37) in Eq. (35), δf_a can be decomposed into two parts:

$$\delta f_a = \delta f_a^{\text{iso}} + \delta f_a^{\text{aniso}}. \qquad (38)$$

The first term on the right hand side is

$$\delta f_a^{\text{iso}} = \frac{\tau_a}{p^\mu u_\mu}f_a^0(1 - f_a^0)\left[p^\mu p^\nu \beta(u_\mu Du_\nu + \nabla_\mu u_\nu)\right.$$
$$\left. + p^\mu(p^\mu u_\mu)(u_\mu D\beta + \nabla_\mu \beta) + \frac{dm_a^2}{dT^2}DT\right]. \quad (39)$$

Employing the equation of motion in ideal hydrodynamics and ideal thermodynamic relations, δf_a^{iso} can be rewritten as

$$\delta f_a^{\text{iso}} = \frac{\tau_a}{p^\mu u_\mu}f_a^0(1 - f_a^0)\left\{\frac{p^\mu p^\nu}{T}\sigma_{\mu\nu}\right.$$
$$\left. + \left[((p^\mu u_\mu)^2 - T^2\frac{dm_a^2}{dT^2})c_s^2 + \frac{1}{3}\Delta_{\mu\nu}p^\mu p^\nu\right]\frac{\theta}{T}\right\}(40)$$

with $\theta = \partial_\alpha u^\alpha$ and c_s^2 being the expansion rate of the fluid and squared sound velocity in the medium, respectively. The velocity stress tensor has the usual definition: $\sigma^{\mu\nu} = \frac{1}{2}\Delta^{\mu\alpha}\Delta^{\nu\beta}(\nabla_\alpha u_\beta + \nabla_\beta u_\alpha - \frac{1}{3}\Delta^{\mu\nu}\theta)$. After tedious

calculations, one can obtain the second term in Eq. (38):

$$\delta f_a^{\text{aniso}} = \frac{(p^\nu V_\nu)^2 \xi \beta}{2p^\nu u_\nu}(2f_a^0 - 1)\delta f_a^{\text{iso}}$$
$$- \frac{(p^\nu V_\nu)^2 \xi}{2(p^\nu u_\nu)^2}\left[p^\mu p^\nu \beta(u_\mu Du_\nu + \nabla_\mu u_\nu)\right.$$
$$\left. - p^\mu(p^\mu u_\mu)(u_\mu D\beta + \nabla_\mu \beta) - \frac{dm_a^2}{dT^2}DT\right]$$
$$\times \frac{\tau_a}{p^\mu u_\mu}f_a^0(1 - f_a^0)$$
$$= \frac{(p^\nu V_\nu)^2 \xi \beta}{2p^\nu u_\nu}(2f_a^0 - 1)\delta f_a^{\text{iso}}$$
$$- \frac{(p^\nu V_\nu)^2 \xi}{2(p^\nu u_\nu)^2}\frac{\tau_a}{p^\mu u_\mu}f_a^0(1 - f_a^0)\left\{\frac{p^\mu p^\nu}{T}\sigma_{\mu\nu}\right.$$
$$\left. - \left[((p^\mu u_\mu)^2 - T^2\frac{dm_a^2}{dT^2})c_s^2 + \frac{1}{3}\Delta_{\mu\nu}p^\mu p^\nu\right]\frac{\theta}{T}\right\}. \quad (41)$$

Allowing the system to be slightly out of equilibrium, the energy-momentum tensor $T^{\mu\nu}$ can be expanded as $T^{\mu\nu} = T_0^{\mu\nu} + T_{\text{diss}}^{\mu\nu}$, where $T_0^{\mu\nu}$ is the ideal perfect fluid form and $T_{\text{diss}}^{\mu\nu}$ is the dissipative part of the energy-momentum tensor. In the hydrodynamical description of hot QCD matter, the dissipative part of the energy-momentum tensor up to the first order in the gradient expansion has the following form [111]:

$$T_{\text{diss}}^{\mu\nu} = \pi^{\mu\nu} - \Pi\Delta^{\mu\nu}, \qquad (42)$$

where $\pi^{\mu\nu}$ and Π are the shear stress tensor and bulk viscous pressure, respectively. In present work, our focus is the shear viscosity component only. In the kinetic theory, the first-order shear stress tensor $\pi^{\mu\nu}$ can be constructed in terms of the distribution functions

$$\pi^{\mu\nu} = \int \frac{d^3\mathbf{p}}{(2\pi)^3}\frac{1}{u \cdot p}\Delta_{\phi\gamma}^{\mu\nu}p^\phi p^\gamma \delta f. \qquad (43)$$

Here, the double projection operator is defined as $\Delta_{\phi\gamma}^{\mu\nu} = \frac{1}{2}(\Delta_\phi^\mu \Delta_\gamma^\nu + \Delta_\gamma^\mu \Delta_\phi^\nu) - \frac{1}{3}\Delta^{\mu\nu}\Delta^{\phi\gamma}$, which can project any rank-2 Lorentz tensor onto its transverse (to u^μ) and traceless part. Inserting Eqs. (38)–(41) to Eq. (43) and comparing with the first-order Navier–Stokes equation $\pi^{\mu\nu} = 2\eta\sigma^{\mu\nu}$ [112], in the rest frame of the thermal system with $u^\mu \equiv (1, \mathbf{0})$ and $p^\nu u_\nu = E_a$, we finally obtain the expression of the ξ-dependent shear viscosity of particle species a,

$$\eta_a = -\frac{\xi d_a}{180T^2}\int \frac{dp}{\pi^2}\frac{\tau_a p^8}{E_a^3}f_a^0(1 - f_a^0)(1 - 2f_a^0 + \frac{T}{E_a}),$$
$$+ \frac{d_a}{30T}\int \frac{dp}{\pi^2}\frac{\tau_a p^6}{E_a^2}f_a^0(1 - f_a^0), \qquad (44)$$

which is consistent with the result from Ref. [92]. For a system consisting of multiple particle species, the total shear viscosity is given as $\eta = \sum_a \eta_a$. For SU(2) light quark matter, $a = u, d, \bar{u}, \bar{d}$ and the spin-color degeneracy factor reads explicitly as $d_a = 2N_c$.

B. Electrical conductivity and Seebeck coefficient

We also investigate the effect of momentum anisotropy on the electrical conductivity and thermoelectric coefficient. Under the RTA, the relativistic Boltzmann–Vlasov equation for the distribution function of single-quasiparticle of charge e_a in the presence of an external electromagnetic field is given by

$$\left[p^\mu \partial_\mu + \left(\frac{1}{2} \partial^\mu m_a^2 + e_a F^{\mu\nu} p_\nu \right) \partial_\mu^{(p)} \right] f_a = -\frac{p^\mu u_\mu \delta f_a}{\tau_a}, \tag{45}$$

where $F^{\mu\nu}$ is the electromagnetic field strength tensor. We only consider the presence of an external electric field, $F^{i0} = -F^{0i} = \mathcal{E} = (\mathcal{E}, 0, 0)$. It is convenient to work in the local rest frame of plasma, and under the steady state assumption (f_a does not depend on time explicitly, $\frac{\partial f_a}{\partial t}$=0), Eq. (45) can be given by [84]

$$\mathbf{v}_a \cdot \nabla f_a + (e_a \mathcal{E} - \nabla E_a) \cdot \frac{\partial f_a}{\partial \mathbf{p}} = -\frac{\delta f_a}{\tau_a}, \tag{46}$$

where we have used of the chain rule $\frac{\partial p^0}{\partial \mathbf{p}} \frac{\partial}{\partial p^0} + \frac{\partial}{\partial \mathbf{p}} \to \frac{\partial}{\partial \mathbf{p}}$. e_a is the electric charge of particle species a, and $\mathbf{v}_a = \partial E_a / \partial \mathbf{p}$ is its velocity. To solve Eq. (46), we assume that the deviation of the distribution function in an anisotropic medium satisfies the following linear form:

$$\delta f_a = -\tau_a (e_a \mathcal{E} - \frac{\partial E_a}{\partial \mathbf{x}}) \cdot \frac{\partial f_a^{\text{aniso}}}{\partial \mathbf{p}} - \tau_a \mathbf{v}_a \cdot \frac{\partial f_a^{\text{aniso}}}{\partial \mathbf{x}}, \tag{47}$$

The spatial gradient of the equilibrium isotropic distribution $\partial_\mathbf{x} f_a^0$ in the presence of a medium-dependent quasiparticle mass can be expressed in the following linear form:

$$\partial_\mathbf{x} f_a^0 = -f_a^0 (1 - f_a^0) \left(\partial_\mathbf{x} (\frac{E_a}{T}) - \partial_\mathbf{x} (\frac{\mu_a}{T}) \right), \tag{48}$$

where $\mu_a = t_a \mu$ denotes the chemical potential of particle species a and $t_a = +1(-1)$ for the quark (antiquark). Considering μ to be homogeneous in space and a temperature gradient only existing along the x-axis, and inserting Eq. (47) into Eq. (46), the perturbative term δf_a in an anisotropic medium can then be written as

$$\delta f_a = H_a \tau_a (e_a \mathcal{E} v_x) - G_a \tau_a \partial_x (\frac{\mu_a}{T}) v_x$$
$$- \frac{\xi(\mathbf{p} \cdot \mathbf{n})^2}{E_a T} f_a^0 (1 - f_a^0) \tau_a \partial_x E_a. \tag{49}$$

The expressions of H_a and F_a in the above equation are as follows, respectively:

$$H_a = \frac{1}{T} f_a^0 (1 - f_a^0)(1 + \xi c(\theta, \phi, \chi))$$
$$- \frac{\xi p^2 c(\theta, \phi, \chi)}{2 E_a T^2} f_a^0 (1 - f_a^0) \left(1 - 2f_a^0 + \frac{T}{E_a} \right), \tag{50}$$

$$G_a = \frac{1}{T^2} f_a^0 (1 - f_a^0) - \frac{\xi p^2 c(\theta, \phi, \chi)}{2 E_a T^3} (E_a - \mu_a)$$
$$\times f_a^0 (1 - f_a^0) \left(1 - 2f_a^0 - \frac{T}{E_a - \mu_a} \right). \tag{51}$$

In the linear response theory, the general formula for the electric current density $\mathbf{J}_a$ due to particle species a in response to an external electric field ($\mathcal{E}$) and temperature gradient ($\nabla_x T$) is given by [113]

$$\mathbf{J}_a = \sigma_{\text{el},a}(\mathcal{E} - S_a \nabla_x T), \tag{52}$$

where $\sigma_{\text{el},a}$ and S_a are the electrical conductivity and Seebeck coefficient of the a-th particle, respectively. In terms of the distribution function, $\mathbf{J}_a$ within the kinetic theory can be written as

$$\mathbf{J}_a = e_a d_a \int \frac{d^3 \mathbf{p}}{(2\pi)^3} \mathbf{v}_a \delta f_a. \tag{53}$$

Finally, the expressions for $\sigma_{\text{el},a}$ and S_a in the weakly anisotropic medium are respectively obtained as follows:

$$\sigma_{\text{el},a} = \frac{e_a^2 d_a \tau_a}{6T} \int \frac{dp}{\pi^2} \frac{p^4}{E_a^2} f_a^0 (1 - f_a^0) \left(1 + \frac{\xi}{3} \right)$$
$$- \frac{\xi e_a^2 d_a \tau_a}{36 T^2} \int \frac{dp}{\pi^2} \frac{p^6}{E_a^3} f_a^0 (1 - f_a^0) \left(1 - 2f_a^0 + \frac{T}{E_a} \right), \tag{54}$$

and

$$S_a = \frac{1}{\sigma_{\text{el},a}} \left[\frac{e_a d_a \tau_a}{6 T^2} \int \frac{dp}{\pi^2} \frac{p^4}{E_a^2} (E_a - \mu_a) f_a^0 (1 - f_a^0) \right.$$
$$- \frac{e_a d_a \xi \tau_a}{36 T^3} \int \frac{dp}{\pi^2} \frac{p^6}{E_a^3} (E_a - \mu_a) f_a^0 (1 - f_a^0)$$
$$\left. \times \left(1 - 2f_a^0 - \frac{T}{(E_a - \mu_a)} \right) \right] = \frac{\alpha_a}{\sigma_{\text{el},a}}, \tag{55}$$

where α_a is the thermoelectric conductivity due to particle species a. In the isotropic limit $\xi \to 0$, Eqs. (54)–(55) reduce to the formulae in the equilibrium. In condensed physics, a semiconductor can exhibit either electron conduction (negative thermopower) or hole conduction (positive thermopower). The total thermopower in a material with different carrier types is given by the sum of these two contributions weighted by their respective electrical conductivity values [114, 115]. Inspired by this, the total Seebeck coefficient in a medium composed of light quarks and antiquarks can be given as

$$S = \frac{\sum_a S_a \sigma_{\text{el},a}}{\sum_a \sigma_{\text{el},a}} = \frac{\sum_a \alpha_a}{\sum_a \sigma_{\text{el},a}} = \frac{\alpha}{\sigma_{\text{el}}}, \tag{56}$$

where the fractional electric charges of up and down (anti-)quarks are given explicitly by $e_u = -e_{\bar{u}} = 2e/3$ and $e_d = -e_{\bar{d}} = -e/3$, where the electric charge reads $e = (4\pi\alpha_s)^{1/2}$ with the fine structure constant $\alpha_s \simeq 1/137$.

VI. COMPUTATION OF THE RELAXATION TIME

To quantify the transport coefficients, one needs to specify the relaxation time. In present work, the scattering processes of (anti)quarks through the exchange of mesons are encoded into the estimation of the relaxation time. The relax-
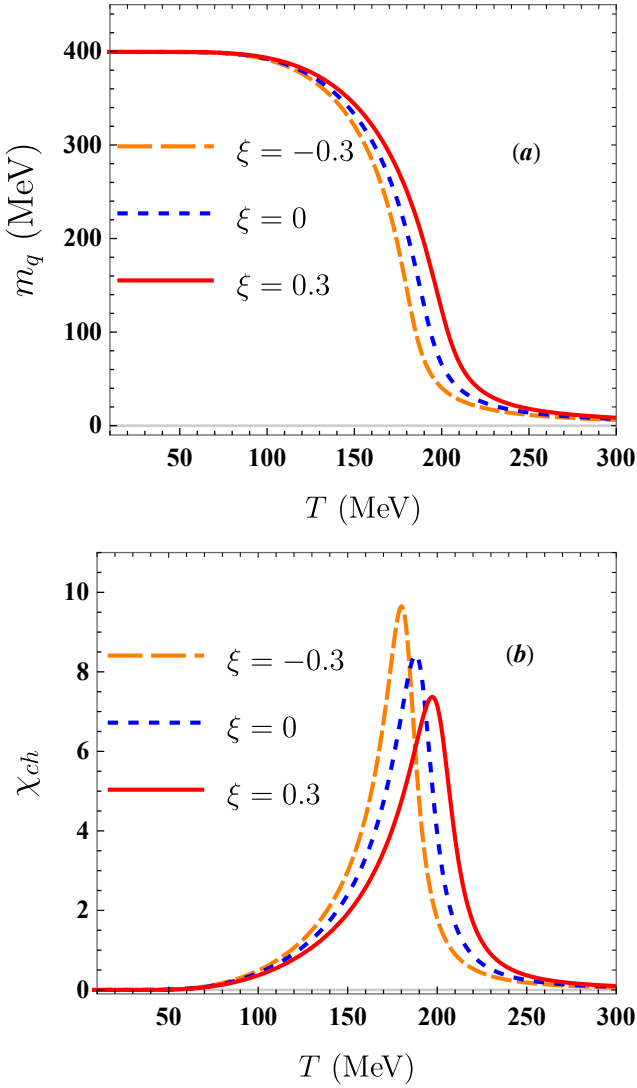
Fig. 1. (Color online) (a) Temperature dependence of the constituent quark mass m_q at $\mu = 0$ MeV for different fixed anisotropy parameters. (b) Chiral susceptibility χ_{ch} at $\mu = 0$ MeV for different fixed anisotropy parameters. The broad dashed lines, dashed lines, and solid lines correspond to the results for $\xi = -0.3$, $\xi = 0$, and 0.3, respectively.

ation times of (anti)quarks are microscopically determined by the thermal-averaged elastic scattering cross section and particle density. For light quarks, the relaxation time in the RTA can be written as [57]

$$\tau_l^{-1}(T,\mu) = n_{\bar{q}}[\bar{\sigma}_{u\bar{u}\to u\bar{u}} + \bar{\sigma}_{u\bar{u}\to d\bar{d}} + \bar{\sigma}_{u\bar{d}\to u\bar{d}}] \\ + n_q[\bar{\sigma}_{ud\to ud} + \bar{\sigma}_{uu\to uu}], \quad (57)$$

where the number density of (anti-)quarks in a weakly anisotropic medium is given as $n_{q(\bar{q})} = d_l \int \frac{d^3 p}{(2\pi)^3} f_{q(\bar{q})}^{an}$, with $d_l = d_{\bar{l}} = 2N_c$ denoting the degeneracy factor. The momenta of the colliding particles for the elastic scattering process $a(\mathbf{p_1}) + b(\mathbf{p_2}) \to c(\mathbf{p_3}) + d(\mathbf{p_4})$ obey the relation $\mathbf{p_1} + \mathbf{p_2} = \mathbf{p_3} + \mathbf{p_4} = \mathbf{0}$, and we use the notation

$|\mathbf{p_1}| = |\mathbf{p_2}| = p$ for convenience. In the center-of-mass (cm) frame, the Mandelstam variables s, t, u are given by

$$s = 4m_q^2 + 4p^2, t = -2p^2(1 - \cos\theta_p),$$
$$u = -2p^2(1 + \cos\theta_p), \quad (58)$$

where θ_p is the scattering angle in the c.m. frame. The Mandelstam variables hold the relation $u + s + t = 4m_q^2$. $\bar{\sigma}_{ab\to cd}$ denotes the thermal-averaged elastic scattering cross section in the weakly anisotropic system, which can be written as

$$\bar{\sigma}_{ab\to cd} = \int_{s_0}^\infty ds \int_{t_{\min}}^{t_{\max}} dt \frac{d\bar{\sigma}_{ab\to cd}}{dt} \sin^2\theta_p \int_{-1}^1 dx_3$$
$$\times (1 - f_c^{\text{aniso}}(p_{\text{cm}}, \mu, x_3)) \int_{-1}^1 dx_4$$
$$\times (1 - f_d^{\text{aniso}}(p_{\text{cm}}, \mu, x_4)) \mathcal{L}(s, \mu, x_1, x_2), \quad (59)$$

with $(1 - f_{c,d}^{\text{an}})$ denoting the Pauli-blocking factor for the fermions due to the fact that some of the final states are already occupied by other identical (anti-)quarks. $\frac{d\bar{\sigma}}{dt} = \frac{1}{16\pi s(s-4m_q^2)}|\bar{M}|^2$ is the differential scattering cross section, with $|\bar{M}|^2$ denoting the squared matrix element of a specific scattering process. The formulae of the squared matrix elements for various scattering processes are presented in the Appendix. The integration limits of t are $t_{\max} = 0$ and $t_{\min} = -4p_{\text{cm}}^2 = -(s - 4m_q^2)$, with $p_{\text{cm}} = (\sqrt{s - 4m_q^2})/2$ denoting the momentum in the c.m. frame. The kinematic boundary of s reads $s_0 = 4m_q^2$. The scattering weighting factor $\sin^2\theta_p = \frac{-4t(s+t-4m_q^2)}{(s-4m_q^2)^2}$ is introduced to exclude the scattering processes with a small initial angle because the large angle scattering dominates in the momentum transport process [116]. In the c.m. frame, the leading-order anisotropic distribution function can be rewritten as

$$f^{\text{aniso}}(p_{\text{cm}}, \mu, x) = f^0(p_{\text{cm}}, \mu)$$
$$- \frac{p_{\text{cm}}^2 \xi x^2}{2E_{\text{cm}}T} f^0(p_{\text{cm}}, \mu)(1 - f^0(p_{\text{cm}}, \mu)), \quad (60)$$

where $E_{\text{cm}} = \frac{s - m_q^2 + m_q^2}{2\sqrt{s}} = \sqrt{s}/2$. In Eq. (59), $\mathcal{L}$ denotes the probability of finding a quark-(anti)quark pair with the center of mass energy $\sqrt{s}$ in the anisotropic medium, and it is given by

$$\mathcal{L} = C\sqrt{s(s - 4m_q^2)} f_a^{\text{aniso}}(p_{cm}, \mu, x_1) f_b^{\text{aniso}}(p_{cm}, \mu, x_2)$$
$$\times v_{\text{rel}}(s), \quad (61)$$

where $v_{\text{rel}}(s) = \sqrt{\frac{s - 4m_q^2}{s}}$ is the relative velocity between two incoming particles in the c.m. frame; C is the normalization constant, which is determined from the requirement that $\int_{s_0}^\infty ds \int_{-1}^1 dx_1 \int_{-1}^1 dx_2 \mathcal{L} = 1$, where $x_1 = \cos\theta_1$ and $x_2 = \cos\theta_2$, with θ_i being the angle between $\mathbf{p}_i$ and $\mathbf{n}$ and $x_1 \equiv -x_3$, $x_2 \equiv -x_4$. Applying the above formula of relaxation time to Eqs. (44), (54), and (55), we can calculate the transport coefficients in the QCD medium and study their sensitivity to the momentum anisotropy.
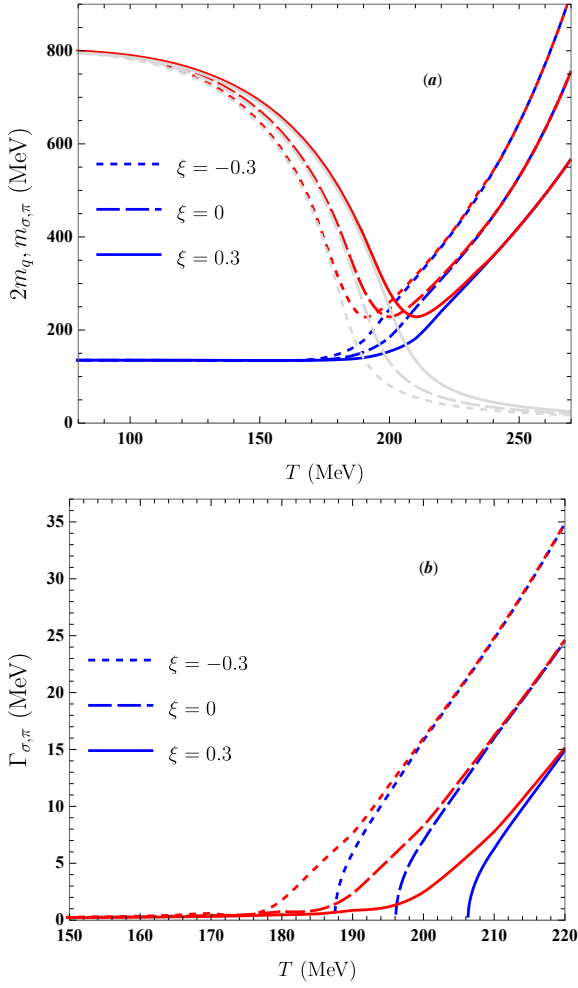
Fig. 2. (Color online) (a) Double mass of the constituent quarks $2m_q$ (gray lines), π meson mass (blue lines), and σ meson mass (red lines) as a function of temperature at $\mu = 0$ GeV for different anisotropy parameters ξ. (b) Temperature dependences of π (blue lines) and σ (red lines) meson decay widths for different ξ. The long dashed lines, dashed lines, and solid lines represent the results for $\xi = -0.3$, $\xi = 0$, and 0.3, respectively, with the corresponding Mott temperatures approximately given by 187 MeV, 196 MeV, and 206 MeV.

VII. RESULTS AND DISCUSSION

Throughout this work, the following parameter set is used: $m_0 = m_{0,u} = m_{0,d} = 5.6$ MeV, $G\Lambda^2 = 2.44$ and $\Lambda = 587.9$ MeV. These values are taken from Ref. [117], where these parameters are determined by fitting quantities in the vacuum ($T = \mu = 0$ MeV). At $T = 0$, the chiral symmetry is spontaneously broken and one obtains the current pion mass $m_{0,\pi} = 135$ MeV, pion decay constant $f_\pi = 92.4$ MeV, and quark condensate $-\langle\psi\psi\rangle^{1/3} = 241$ MeV.

In the NJL model, the constituent quark mass is a good indicator and an order parameter for analyzing the dynamical feature of chiral phase transition. In the asymptotic expansion-driven momentum anisotropic system, the

anisotropy parameter ξ is always positive owing to the rapid expansion along the beam direction. However, in the presence of a strong magnetic ξ, it becomes negative because of the reduction in transverse momentum due to Landau quantization. As we restrict the analysis to only a weakly anisotropic medium, the anisotropy parameter we address here is artificially taken as $\xi = -0.3$, 0.0, 0.3 to investigate phenomenologically the effect of ξ on various quantities. In Fig. 1 (a), we show the thermal behavior of the light constituent quark mass m_q for vanishing quark chemical potential at different ξ. For low temperature, m_q remains approximately constant at ($m_q \approx 400$ MeV), and then, with increasing temperature m_q, it continuously drops to near zero. The transition to small mass occurs at higher temperature for a higher value of ξ. These phenomena imply that at zero chemical potential, the restoration of the chiral symmetry (the chiral symmetry is not strictly restored because the current quark mass is nonzero) in an (an-)isotropic quark matter takes place as crossover phase transition, and an increase in ξ can lead to a catalysis of chiral symmetry breaking.

In this work, the chiral critical temperature, T_c, was determined by the peak location of the associated chiral susceptibility χ_{ch}, which is defined as $\chi_{ch} = \left|\frac{dm_q}{dT}\right|$. We stress that the criterion of obtaining the chiral critical temperature is different in different studies. Because of some shortcomings of the NJL model, such as parameter ambiguity, nonrenormalization, and the absence of gluonic dynamics, the value of T_c in the present work is not expected to describe the lattice QCD result quantitatively. However, these shortcomings cannot affect our present qualitative results. The temperature dependence of chiral susceptibility χ_{ch} for different ξ at $\mu = 0$ MeV is plotted in Fig. 1 (b). We observe that T_c exhibits a significant ξ dependence. As ξ increases, T_c shifts toward higher temperatures and the height of the peak decreases. The locations of T_c for $\xi = -0.3$, 0, 0.3 are $\sim$ 180 MeV, 188 MeV, and 197 MeV, respectively, which means a change of approximately 10% in temperature. Actually, the in-medium meson masses also can be regarded as a signature of chiral phase transition. In Fig. 2(a), we display the variation of π and σ meson masses with temperature for different ξ at $\mu = 0$ MeV. As can be observed, the π mass remains approximately constant up to a particular temperature whereas the σ mass first decreases and then increases. As temperature increases further, the difference between the π mass and σ mass decreases and finally vanishes, where σ and π mesons are degenerate and become nonphysical degrees of freedom, which indicates the restoration of chiral symmetry. Further, before π and σ meson masses emerge, the π mass decreases as ξ increase beyond T_c, whereas the σ mass first increases and then decreases with the increase in ξ. Our result slightly differs from that in Ref [40], in which the NJL model is used for a quark matter of finite size. The study shows that below the critical temperature, the π mass enhances as the system size decreases, whereas the σ mass first remains unchanged and then increases. We also see that at a certain temperature, the double constituent quark mass ($2m_q$) is equal to the π mass, so the pion meson is no longer a bound state but only a $q\bar{q}$ resonance and obtains a finite de-
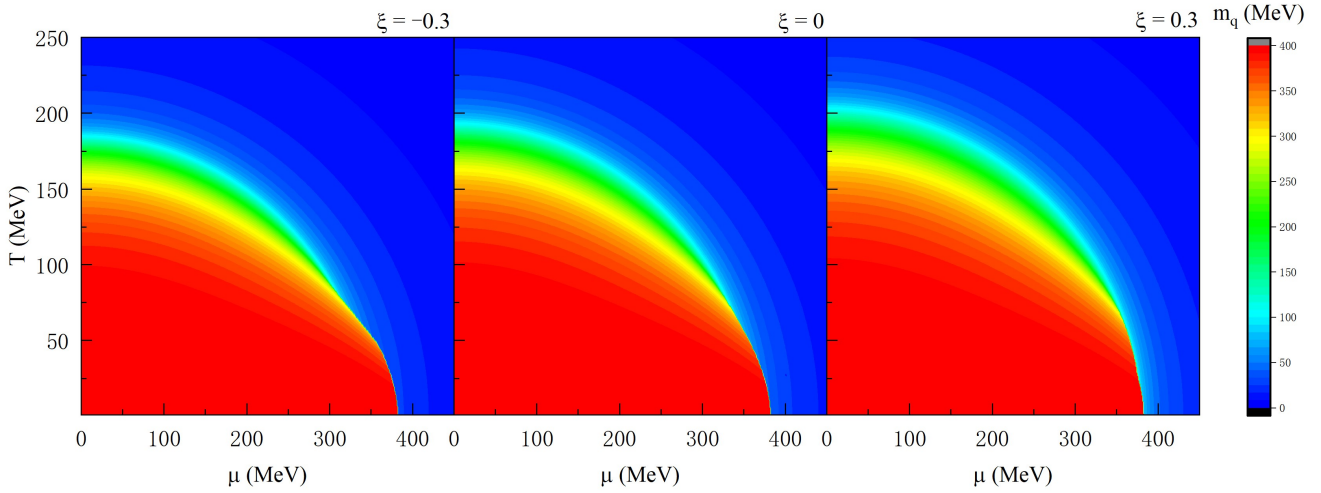
Fig. 3. (Color online) Three-dimensional plot of the constituent quark mass m_q with respect to temperature and quark chemical potential for different anisotropy parameters ($\xi = -0.3,\ 0,\ 0.3$).
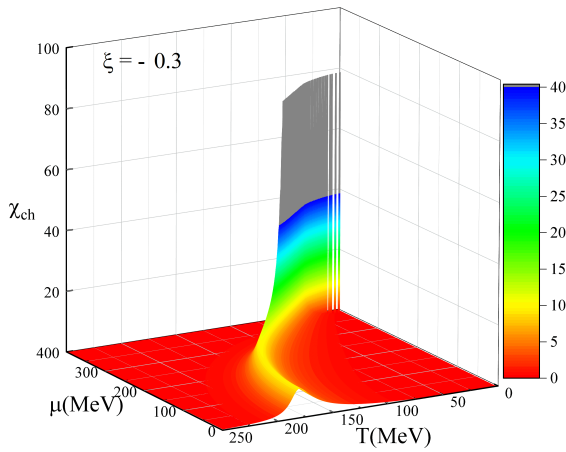

Fig. 4. (Color online) Three-dimensional plot of chiral susceptibility χ_{ch} for $\xi = -0.3$ in the entire μ and T ranges of interest. The gray area means that χ_{ch} is divergent. The values remain finite due to numerical problems (differential quotient). The peak height at high μ is two orders of magnitude higher than that in cases with low μ and can be considered "divergent".
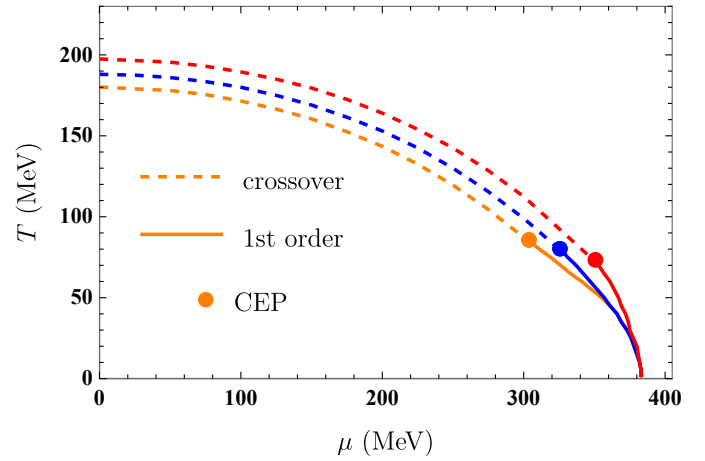

Fig. 5. (Color online) Chiral phase diagram for different anisotropy parameters in the Nambu–Jona–Lasinio (NJL) model. The inside curve is for $\xi = -0.3$, the next curve is for $\xi = 0$, and the outermost curve is for $\xi = 0.3$. The solid lines denote the first-order phase transition curves, the dashed lines denote the crossover transition curves, and the solid dots represent the critical endpoints (CEPs). We observe that the CEP is shifted towards larger values of the quark chemical potential but smaller values of the temperature for higher anisotropy parameters.

cay width. Accordingly, the Mott transition temperature by the definition $m_\pi(T_{\text{Mott}}) = 2m_q(T_{\text{Mott}})$ can be obtained. The Mott temperatures for $\xi = -0.3,\ 0$, and 0.3 turn out to be $\sim$ 187 MeV, 196 MeV, and 206 MeV, respectively, which are slightly higher than the corresponding T_c. In the vicinity of the Mott temperature, the σ meson features its minimal mass. In Fig. 2 (b), we illustrate the variation in the decay widths of both σ and π mesons with temperature for different ξ. As can be observed, the decay width of the σ meson, Γ_σ, is finite in the entire temperature range whereas the decay width of the π meson, Γ_π, starts after the Mott temperature. At high temperature, the merging behaviors of the decay widths for different

mesons are also observed. With the increase in ξ, the decay widths of mesons are reduced.

We continue the analysis in the finite quark chemical potential case to investigate the effect of momentum anisotropy on the phase boundary and CEP position. First, we display the temperature- and quark chemical potential-dependence of constituent quark mass m_q for different anisotropy parameters, as shown in Fig. 3. We can observe that at a small μ, m_q continuously decreases with increasing T, whereas m_q has a significant discontinuity or a sharp drop along the T-axis at sufficiently high μ, which is usually considered as

Fig. 7. (Color online) Relaxation time of quarks at $\mu = 0$ MeV as a function of temperature for different anisotropy parameters, i.e., $\xi = -0.3$ (orange long dashed line), $\xi = 0$ (blue dashed line), and $\xi = 0.3$ (red solid line).
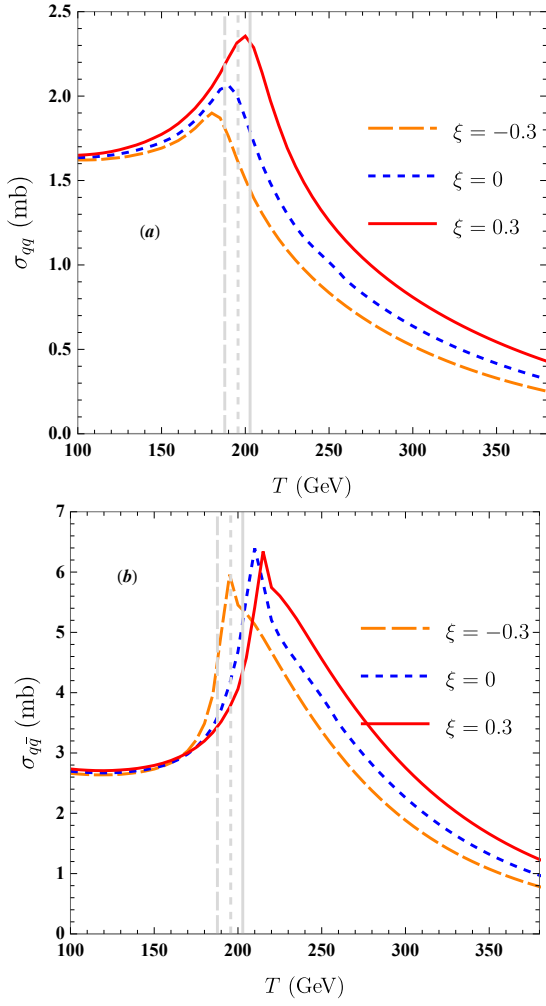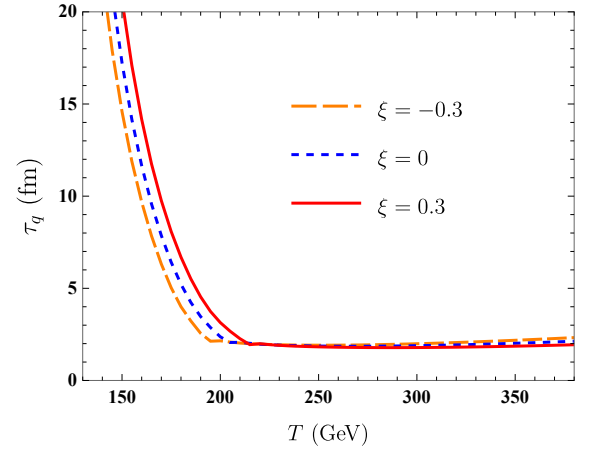
Fig. 6. (Color online) (a) Total cross section of the quark–quark scattering processes $\bar{\sigma}_{qq}$ as a function of temperature at $\mu = 0$ MeV for different anisotropy parameters. (b) The total cross section of quark-antiquark scattering processes $\bar{\sigma}_{q\bar{q}}$ as a function of temperature at $\mu = 0$ MeV for different anisotropy parameters, i.e., $\xi = -0.3$ (orange long dashed line), $\xi = 0$ (blue dashed line), and $\xi = 0.3$ (red solid line). The gray vertical lines (from left to right) represent the critical temperatures $T_c = 180$ MeV, 188 MeV, and 197 MeV for $\xi = -0.3$, 0, 0.3, respectively.

the appearance of a first-order phase transition. To visualize the phase diagram, we use the significant divergency of χ_{ch} at sufficiently high chemical potential as the criterion for a first-order phase transition, as shown in Fig. 4. With the decrease in μ, the first-order phase transition terminates at a CEP, where the phase transition is expected to be of second order. As μ decreases further, the maximum of the chiral susceptibility (χ_{ch}) as the crossover criterion. The full chiral boundary lines in the (μ-T) plane for three different values of ξ are displayed in Fig. 5. We observe that as ξ increases, the phase boundary shifts toward higher quark chemical potentials and higher temperatures. We observe that the CEP appears in the low temperature and high chemical potential regions. Once the effect of momentum

anisotropy ($\xi > 0$) is taken into account, the rapid expansion and fast cooling of the created fireball along the beam direction make the temperature of the anisotropic system lower than that of the isotropic system under the same conditions. By modifying the distribution function in the gap equation, we can study the influence of momentum anisotropy on the position of the CEP. It is noted that the criteria for determining the CEP position remain the same for both isotopic and anisotropic systems. Therefore, as ξ increases, the momentum component (temperature) in the anisotropic distribution function $f^{iso}(\sqrt{\mathbf{p}^2 + \xi(\mathbf{p} \cdot \mathbf{n})^2})$ increases (decreases). Accordingly, the chemical potential in the anisotropic function for determining the CEP position is greater than that in the isotropic distribution function. The CEP locations (T_{CEP}, μ_{CEP}) in this work are presented at (298.70 MeV, 88.2 MeV), (321.8 MeV, 82.4 MeV), (348.4 MeV, and 74.2 MeV) for $\xi = -0.3$, 0, 0.3, respectively. The position of the CEP for $\xi = 0$ in this work is almost consistent with the existing result [118] for the same parameter set. The value of μ_{CEP} (T_{CEP}) from $\xi = -0.3$ to $\xi = 0.3$ increases (decreases) by approximately 16% (17%), indicating that the influence degree of momentum anisotropy on the temperature of the CEP is almost the same as that on the quark chemical potential of the CEP. This is different from the effect due to the finite volume in Ref. [38], which has indicated that in the PNJL model, the finite volume affects the CEP shift along the temperature stronger than along the quark chemical potential shift. When the system size is reduced to 2 fm, the CEP in the PNJL model vanishes and the whole chiral phase boundary becomes a crossover curve. Based on this result, there also exists a possibility that if ξ further increases, the CEP may disappear from the phase diagram.

To better understand the qualitative behavior of the transport coefficients in the quark matter, we first discuss the results of the scattering cross sections and the relaxation time. In Fig 6, we display the total cross section of quark–quark scattering processes $\bar{\sigma}_{qq} = \bar{\sigma}_{uu \to uu} + \bar{\sigma}_{ud \to ud}$ (plot
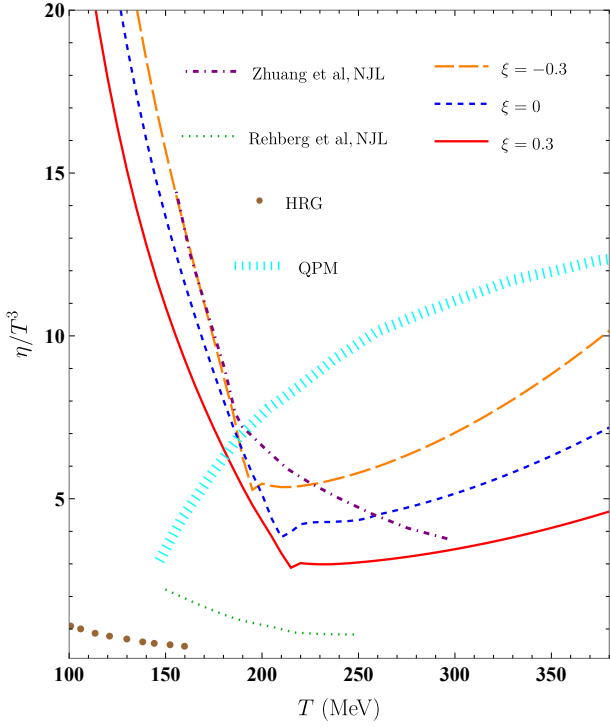
Fig. 8. (Color online) Temperature dependence of scaled shear viscosity η/T^3 in quark matter at vanishing chemical potential for different anisotropy parameters, i.e., $\xi = -0.3$ (orange long dashed line), $\xi = 0$ (blue dashed line), and $\xi = 0.3$ (red solid line). The thick cyan dotted line represents the result in the $N_f = 3$ quasiparticle model (QPM) [59], which is an effective model for the description of non-perturbative QCD. The purple dash-dotted line shows the result obtained in the $N_f = 2$ NJL model by Zhuang et al. [57]. The brown dots show the result from hadron resonance gas (HRG) model [70]. The green dots correspond to the result of Rehberg et al. in the $N_f = 3$ NJL model [58] using the averaged transition rate method for the estimation of relaxation time.

Fig. 9. (Color online) Temperature dependence of scaled electrical conductivity σ_{el}/T in quark matter at vanishing chemical potential for different anisotropy parameters, i.e., $\xi = -0.3$ (orange long dashed line), $\xi = 0$ (blue dashed line), and $\xi = 0.3$ (red solid line). The green dotted line shows the result of Marty et al. in the $N_f = 3$ NJL model [54]. The thick gray dash-dotted line represents the result from the pQCD-based microscopic Boltzmann approach to multi-parton scatterings (BAMPS) transport model [67] with running coupling constant. The brown stars present the result in the parton-hadron-string dynamics (PHSD) transport approach [66]. The cyan dotdashed line shows the result within the excluded volume hadron resonance gas (EVHRG) model with the RTA [71]. The darkyellow dots are the lattice date obtained from Ref. [69]. The red open circles are the calculation for hadronic gas in the transport approach simulating many accelerated strongly-interacting hadrons (SMASH) [65] based on the Green–Kubo formalism.

a) and the total cross section of quark–antiquark processes $\bar{\sigma}_{q\bar{q}} = \bar{\sigma}_{u\bar{u}\to u\bar{u}} + \bar{\sigma}_{u\bar{d}\to u\bar{d}} + \bar{\sigma}_{u\bar{u}\to d\bar{d}}$ (plot b) as functions of temperature at different anisotropy parameters for vanishing quark chemical potential. As can be observed, $\bar{\sigma}_{qq}$ and $\bar{\sigma}_{q\bar{q}}$ have similar peak structures in their temperature dependence, i.e., the scattering cross sections first increase, reach a peak, and decrease with increasing temperature afterwards. In addition, the magnitude of $\bar{\sigma}_{q\bar{q}}$ is higher than that of $\bar{\sigma}_{qq}$, and this is mainly due to the additional s-channel contribution to a resonance of the exchanged meson with the incoming quark and antiquark, which leads to a large peak in the cross section [74]. We further observe that the scattering cross sections in the weakly anisotropic medium have the same behaviors as those in the isotropic medium. As ξ increases, $\bar{\sigma}_{qq}$ increases in the entire considered temperature domain, whereas $\bar{\sigma}_{q\bar{q}}$ first decreases as ξ increases, and then increases as ξ increases. With an increase in ξ, the maximum of the scattering cross section shifts toward higher temperatures. The location of the maximum for $\bar{\sigma}_{qq}$ at different ξ is nearly in agreement with the respective T_c, as the peak positions of $\bar{\sigma}_{q\bar{q}}$
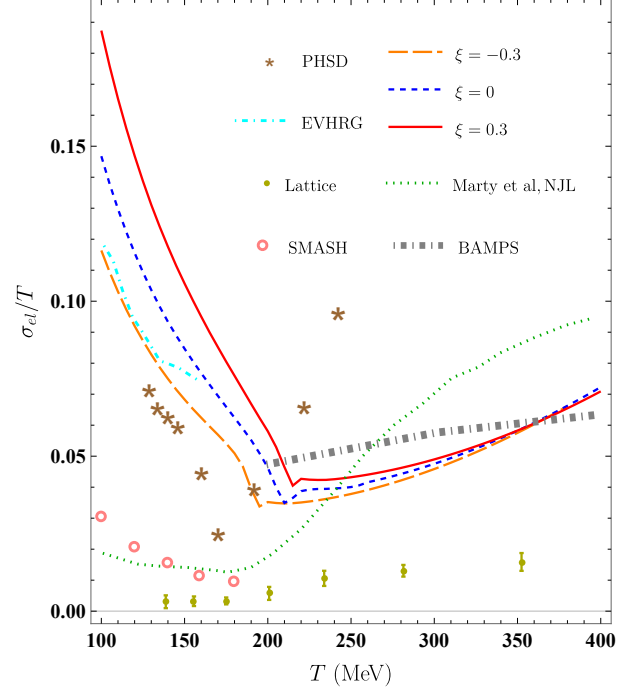
respectively locate at $\sim 1.07\, T_c^{-0.3}$, $1.07\, T_c^0$, $1.10\, T_c^{0.3}$ for $\xi = -0.3$, 0, 0.3, with T_c^{ξ} denoting the chiral critical temperature for a fixed ξ.

The dependence of total quark relaxation time τ_q on temperature for vanishing quark chemical potential at different ξ is displayed in Fig. 7. As can be observed, τ_q first decreases sharply with increasing temperature, and after an inflection point (viz, the peak position of $\bar{\sigma}_{q\bar{q}}$), τ_q changes modestly with temperature. Further, the increase in τ_q with ξ is significant at low temperature, whereas at high temperature the reduction in τ_q with ξ is imperceptible. This is the result of the competition between the quark number density and the total scattering cross section in Eq. (57). At low temperature, the ξ dependence of τ_q is mainly determined by the inverse quark number density, whereas at high temperature it is primarily governed by the inverse total cross section, even though this effect is largely cancelled out by the inverse quark density effect.
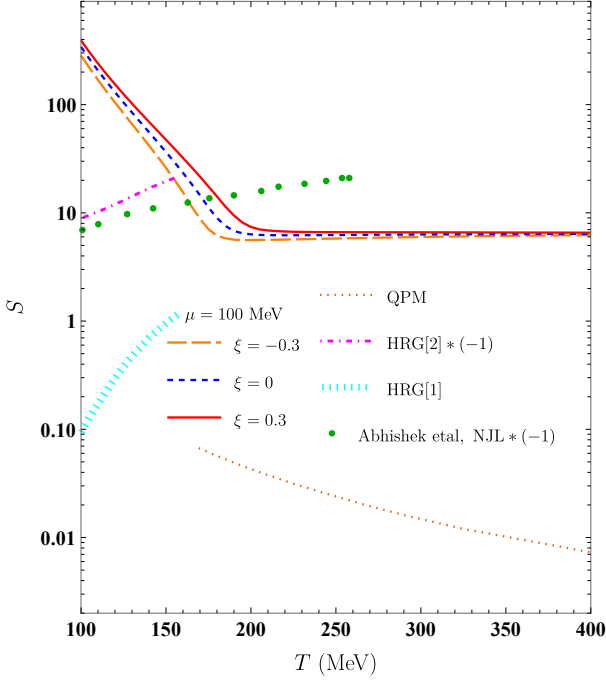
Fig. 10. (Color online) Temperature dependence of the Seebeck coefficient in quark matter at $\mu = 100$ MeV for different anisotropy parameters, i.e., $\xi = -0.3$ (orange broad dashed line), $\xi = 0$ (blue dashed line), and $\xi = 0.3$ (red solid line). The brown dotted line corresponds to the result for the QGP in the quasiparticle model [83] at $\mu_q = 50$ MeV. The cyan thick-dotted line represents the result in the hadron resonance gas model for $\mu_B = 0.1$ GeV [81]. The mauve dash-dotted line and green dots, respectively, represent the results in the HRG model for $\mu_B = 50$ MeV [80] and the $N_f = 2$ NJL model for $\mu = 100$ MeV [84], where the gradient of the quark chemical potential apart from a spatial gradient in temperature is also included.

Next, we discuss the results regarding various transport coefficients. In Fig. 8, the temperature dependence of scaled shear viscosity η/T^3 in quark matter for different momentum anisotropy parameters at a vanishing chemical potential is displayed. We observe that with increasing temperature, η/T^3 first decreases, reaches a minimum around the critical temperature, and increases afterwards. The temperature position for the minimum η/T^3 is consistent with the temperature for the peak $\bar{\sigma}_{q\bar{q}}$. This dip structure of η/T^3 mainly depends on the competition between the quark distribution function f_q^0 and the quark relaxation time τ_q in the integrand of Eq. (44). The decreasing feature of η/T^3 in the low temperature domain is governed by τ_q, whereas in the high temperature domain, the increasing behavior of f_q^0 overwhelms the decreasing behavior of τ_q, resulting in η/T^3 as an increasing function of temperature. In addition, we observe that with an increase in ξ, η/T^3 has an overall enhancement and the minimum of η/T^3 shifts to higher temperatures. This behavior of η/T^3 can be understood from the related expression in Eq. (44), where apart from the ξ-dependent relaxation time, the first term in the integrand of Eq. (44) has an additional ξ factor, which leads to an overall enhancement of the absolute first term at low T. The variation of the first term at low T is larger

than the counterpart of the second term, which results in a suppression of η/T^3 for the inclusion of positive ξ. Meanwhile, at high T, the qualitative and quantitative behavior of η/T^3 with ξ is dominated by the second term. The location of the minimum for η/T^3 at different ξ is consistent with the peak position of $\bar{\sigma}_{q\bar{q}}$. We further observe that η/T^3 decreases as ξ increases in the entire temperature region. In addition, we also compare our result for $\xi = 0$ with the results reported in the literature. The calculation of η/T^3 in the hadron resonance gas (HRG) model [70] (brown dots) using the RTA is a decreasing function with temperature, which is qualitatively similar to ours below the critical temperature. The quantitative difference between the HRG model result and ours can be attributed to the use of different degrees of freedom and scattering cross sections. The result of Zhuang $et\ al$ [57] in the $N_f = 2$ NJL model (purple dash-dotted line) is of the same order of magnitude as ours, whereas at high temperature, their result still has a decreasing feature because an ultraviolet cutoff is used in all momentum integrals whether the temperature is finite or zero. The result estimated in the quasiparticle (QPM) [59] is a logarithmically increasing function of temperature beyond the critical temperature, and it is quantitively larger than ours beyond the critical temperature owing to the differences in both the effective quark mass and relaxation time. The result of Rehberg $et\ al$ [58] for the $N_f = 3$ NJL model in the temperature regime close to the critical temperature is smaller than ours, and the obvious dip structure is not observed because the momentum cutoff is also used at finite temperature.

In Fig. 9, we plot the thermal behavior of scaled electrical conductivity σ_{el}/T at $\mu = 0$ MeV for different ξ. Similar to the temperature dependence of η/T^3, σ_{el}/T also exhibits a dip structure in the entire temperature region of interest. We also present the comparison with other previous results. The result obtained from the PHSD approach [66] (brown stars), where the plasma evolution is solved by a Kadanoff–Baym type equation, also has a valley structure, even though the location of the minimum is different from ours. We also observe that in the temperature region dominated by the hadronic phase, the thermal behavior of σ_{el}/T using the microscopic simulation code SMASH [65] (pink open circles) is similar to ours. Furthermore, our result is much larger than the lattice QCD data (dark yellow dots) taken from Ref. [69] owing to the uncertainty in the parameter set and absence of gluonic dynamics. The result within the excluded volume hadron resonance gas (EVHRG) model [71] (cyan dash-dotted line) and the result obtained from the partonic cascade BAMPS [67] (gray thick dash-dotted line) are qualitatively and quantitively similar to our calculations below the critical temperature and beyond the critical temperature, respectively. Our result is similar to that of Marty et al. obtained within the $N_f = 3$ NJL model [54] (green dotted line), with the numerical discrepancy mainly coming from the differences in the values of the model parameter set and scattering cross sections. At low T, the absolute values of both the first and second terms in Eq. (54) increase as ξ increases. However, the variation of the first term is larger than that of the second term, which results in an enhancement of σ_{el}/T. At high T, the decreasing

feature of relaxation time with ξ can weaken the increasing behavior of σ_{el}/T with ξ, and the values of σ_{el}/T for different ξ gradually approach and eventually overlap. Our qualitative result of σ_{el}/T is different from the result in Ref. [73], where the σ_{el}/T of the QGP is a monotonic decreasing function of ξ. This occurs because the effect of momentum anisotropy is not incorporated in the calculation of the relaxation time and the effective mass of quasiparticles, as the ξ dependence of σ_{el}/T is only determined by the anisotropic distribution function. We also observe that with the increase in ξ, the minimum of σ_{el}/T shifts to higher temperatures, which is similar to η/T^3. However, the height of the minimum increases, which is opposite to η/T^3.

Finally, we study the Seebeck coefficient S in quark–antiquark matter. Owing to the sensitivity of S to the charge of particle species, at a vanishing chemical potential, quark number density n_q is equal to antiquark number density $n_{\bar{q}}$, and the contribution of quarks to S is exactly cancelled by that of antiquarks. Thus, a finite quark chemical potential is required to obtain a non-zero thermoelectric current in the medium. In Fig. 10, we plot the variation of S with respect to temperature for different ξ at $\mu = 100$ MeV. The comparison with other previous calculations, which were all performed in the kinetic theory under the RTA, is also presented. We remind the reader that at finite μ, n_q is larger than $n_{\bar{q}}$, and the contribution of quarks to total S in magnitude is always prominent. As shown in Fig. 10, the sign of S in our investigation is positive, which indicates that the dominant carriers converting the heat gradient to the electric field are positively charged quarks, i.e., up quarks. Actually, the positive or negative sign of S is mainly determined by the factor $(E_q - \mu_q)$ in the integrand of Eq. (55). In Ref. [83], the Seebeck coefficient studied in the QPM (brown dotted line) at $\mu = 50$ MeV also exhibits a decreasing feature with increasing temperature. The result of Abhishek et al [84] at $\mu = 100$ MeV in the $N_{\text{f}} = 2$ NJL model (the green dots) is very different from ours. In Ref. [84], S is negative and its absolute value is an increasing function with temperature. The reasons behind this quantitative and qualitative discrepancy are twofold: (1) the relaxation time in Ref. [84] was estimated using the averaged transition rate $\bar{w}_{ij}$, whereas our relaxation time was obtained from the thermally averaged cross section of elastic scattering (a detailed comparison of the two methods can be found in Ref. [74]); (2) in Ref. [84], the spatial gradient of chemical potential was also included apart from the temperature gradient and accordingly, the sign of S was primarily determined by the factor $(E_q - \omega/n_q)$ with ω denoting the enthalpy density in the associated formalism. Given that the single-particle energy E_q remains smaller than (ω/n_q), S in Ref. [84] is negative. We also observed that with increasing temperature, S sharply decreased below T_{c}, whereas the decreasing feature of S was inconspicuous above T_{c}. Further, the value of S at low T was much larger than that at high T. This is also different from the result in Ref. [84], where the absolute value of S in quark matter increased with increasing temperature because of the increasing behaviors of both the factor $| - \omega/n_q|$ and the equilibrium distribution function. In addition, the Seebeck coefficient in the HRG model [80, 81]

is also positive (negative) without (with) the spatial gradient of chemical potential (cyan thick dotted line and mauve dash-dotted line). Nevertheless, the absolute value of S in hadronic matter is still an increasing function of temperature regardless of the spatial gradient of μ. We also observed that as ξ increases, S has a quantitative enhancement, which is primarily due to a significant rise in the thermoelectric conductivity α, even though $1/\sigma_{\text{el}}$ has a cancellation effect on the increase in S. At sufficiently high temperature, the rise in $1/\sigma_{el}$ can almost compensate the reduction in α, and as a result, S varies insignificantly with the ξ of interest, compared to the value of S itself.

VIII. SUMMARY

We phenomenologically investigated the impact of weak momentum-space anisotropy on the chiral phase structure, mesonic properties, and transport properties of quark matter in the 2-flavor NJL model. The momentum anisotropy, which is induced by the initial preferential expansion of the created fireball in heavy-ion collisions along the beam direction, can be incorporated in the calculation through the parameterization of the anisotropic distribution function. Our result has shown that the chiral phase transition is a smooth crossover for vanishing quark chemical potential, independent of the anisotropy parameter ξ, and an increase in ξ can even hinder the restoration of the chiral symmetry. We found that the CEP is highly sensitive to the change in ξ. With the increase in ξ, the CEP shifts to higher μ and smaller T, and the momentum anisotropy affects the CEP temperature to almost the same degree as it affects the CEP chemical potential. Before the merge of π and σ meson masses, the ξ dependence of the π meson mass is opposite to that of the σ meson mass.

We also studied the thermal behavior of various transport coefficients, such as the scaled shear viscosity η/T^3, scaled electrical conductivity σ_{el}/T, and Seebeck coefficient S at different ξ. The associated ξ-dependent expressions are derived by solving the relativistic Boltzmann–Vlasov transport equation in the relaxation time approximation, and the momentum anisotropy effect is also embedded in the estimate of relaxation time. We found that η/T^3 and σ_{el}/T have a dip structure around the critical temperature. Within the consideration of momentum anisotropy, η/T^3 decreases as ξ increases and the minimum shifts to higher temperatures. With the increase in ξ, σ_{el}/T significantly increases at low temperature, whereas its sensitivity to ξ at high temperature is significantly reduced, which is different from the behavior of η/T^3 with respect to ξ. We also found that the sign of S at $\mu = 100$ MeV was positive, indicating that the dominant carriers for converting the thermal gradient to the electric field are up quarks. With increasing temperature, S first decreases sharply and then almost flattens out. At low temperature, S significantly increases with the increase in ξ, whereas at high temperature the rise is marginal compared to the value of S itself.

We note that it is of considerable interest to include the Polyakov-loop potential in the present model to study both

chiral and confining dynamics in a weakly anisotropic quark matter. A more general ellipsoidal momentum anisotropy characterized by two independent anisotropy parameters is then needed to gain a deeper understanding of the QGP properties. In the present work, no proper time dependence was given to the anisotropy parameter. However, in a realistic case, ξ varies with the proper time starting from the initial proper time up to a time when the system becomes isotropic. Thus, a proper time dependent anisotropy parameter [119] needs to be introduced to better explore the effect of time-dependent momentum anisotropy on chiral phase transition. For the strongly longitudinal expanding QCD matter, the investigation of chiral phase transition needs to be performed by numerically solving both the Vlasov equation and gap equation concurrently and continuously. In this case, the phase diagram of a strongly expanding system is a map in the space–time plane rather than in the $T - \mu$ plane. In addition, the investigation of the thermoelectric coefficients, especially the magneto-Seebeck coefficient and Nernst coefficient in magnetized quark matter, based on the PNJL model would be an

attractive direction, and we plan to work on it in the near future.

APPENDIX

In the $N_f = 2$ NJL model, there are 12 different elastic scattering processes:

$$
\begin{aligned}
&u\bar{u} \to u\bar{u}, \ u\bar{d} \to u\bar{d}, \ u\bar{u} \to d\bar{d}, \\
&uu \to uu, \ ud \to ud, \ \bar{u}\bar{u} \to \bar{u}\bar{u}, \\
&\bar{u}\bar{d} \to \bar{u}\bar{d}, \ d\bar{d} \to d\bar{d}, \ d\bar{d} \to u\bar{u}, \\
&d\bar{u} \to d\bar{u}, \ dd \to dd, \ \bar{d}\bar{d} \to \bar{d}\bar{d}.
\end{aligned} \tag{62}
$$

The explicit expressions of the squared matrix elements for the $u\bar{u} \to u\bar{u}$, $u\bar{d} \to u\bar{d}$, and $ud \to ud$ processes via exchange of scalar and/or pseudoscalar mesons to $1/N_c$ order are given as

$$
|\bar{M}_{u\bar{u}\to u\bar{u}}|^2(s,t) = s^2|D_s^\pi|^2 + t^2|D_t^\pi|^2 + (s-4m^2)^2|D_s^\sigma|^2 + (t-4m^2)^2|D_t^\sigma|^2 + \frac{1}{N_c}Re\left[stD_s^{\pi^*}D_t^\pi + s(4m^2-t)D_s^{\pi^*}D_t^\sigma \right.
$$

$$
\left. + t(4m^2-s)D_t^\pi D_s^{\sigma^*} + (st + 4m^2(s+t) - 16m^4)D_t^\sigma D_s^{\sigma^*}\right], \tag{63}
$$

$$
|\bar{M}_{u\bar{d}\to u\bar{d}}|^2(s,t) = 4s^2|D_s^\pi|^2 + t^2|D_t^\pi|^2 + (t-4m^2)^2|D_t^\sigma|^2 - \frac{1}{N_c}Re\left[2stD_s^{\pi^*}D_t^\pi + 2s(4m^2-t)D_s^{\pi^*}D_t^\sigma\right], \tag{64}
$$

$$
|\bar{M}_{ud\to ud}|^2(t,u) = 4u^2|D_u^\pi|^2 + t^2|D_t^\pi|^2 + (t-4m^2)^2|D_t^\sigma|^2 - \frac{1}{N_c}Re\left[2utD_u^{\pi^*}D_t^\pi + 2u(4m^2-t)D_u^{\pi^*}D_t^\sigma\right]. \tag{65}
$$

The meson propagators in the above processes are ξ-dependent. Based on the above formulae of three scattering processes, the squared matrix element for the remaining scattering processes can be obtained through charge conjugation and crossing symmetry [57, 120].

AUTHOR CONTRIBUTIONS

[1] Z. B. Tang, W. M. Zha, Y. F. Zhang, An experimental review of open heavy flavor and quarkonium production at RHIC. Nucl. Sci. Tech. **31**, 81 (2020). doi:10.1007/s41365-020-00785-8

[2] L. L. Zhu, B. Wang, M. Wang et al., Energy and centrality dependence of light nuclei production in relativistic heavy-ion collisions. Nucl. Sci. Tech. **33**, 45 (2022). doi:10.1007/s41365-022-01028-8

[3] J. H. Gao, G. L. Ma, S. Pu et al., Recent developments in chiral and spin polarization effects in heavy-ion collisions. Nucl. Sci. Tech. **31**, 90 (2020). doi:10.1007/s41365-020-00801-x

[4] Y. C. Liu, X. G. Huang, Anomalous chiral transports and spin polarization in heavy-ion collisions. Nucl. Sci. Tech. **31**, 56 (2020). doi:10.1007/s41365-020-00764-z

[5] Y. C. Liu, X. G. Huang, Spin polarization formula for Dirac fermions at local equilibrium. Sci. China Phys. Mech. Astron. **65**, 272011 (2022). doi:10.1007/s11433-022-1903-8

[6] Y. Aoki, G. Endrodi, Z. Fodor et al., The Order of the quantum chromodynamics transition predicted by the standard model of particle physics. Nature **443**, 675 (2006). doi:10.1038/nature05120

[7] A. Bazavov et al., Equation of state in (2+1)-flavor QCD. Phys. Rev. D **90**, 094503 (2014). doi:10.1103/PhysRevD.90.094503

[8] K. Splittorff, J. J. M. Verbaarschot, The QCD Sign Problem for Small Chemical Potential. Phys. Rev. D **75**, 116003 (2007). doi:10.1103/PhysRevD.75.116003

[9] A. Barducci, R. Casalbuoni, S. De Curtis et al., Chiral Symmetry Breaking in QCD at Finite Temperature and Density. Phys. Lett. B **231**, 463 (1989). doi:10.1016/0370-2693(89)90695-3

[10] M. Asakawa, K. Yazaki, Chiral Restoration at Finite Density and Temperature. Nucl. Phys. A **504**, 668 (1989). doi:10.1016/0375-9474(89)90002-X

[11] R. V. Gavai, S. Gupta, Pressure and nonlinear susceptibilities in QCD at finite chemical potentials. Phys. Rev. D **68**, 034506 (2003). doi:10.1103/PhysRevD.68.034506

[12] C. R. Allton, S. Ejiri, S. J. Hands et al., The Equation of state for two flavor QCD at nonzero chemical potential. Phys. Rev. D **68**, 014507 (2003). doi:10.1103/PhysRevD.68.014507

[13] E. Laermann, F. Meyer, M. P. Lombardo, Making the most of Taylor expansion and imaginary μ. J. Phys. Conf. Ser. **432**, 012016 (2013). doi:10.1088/1742-6596/432/1/012016

[14] O. Philipsen, C. Pinke, The $N_f = 2$ QCD chiral phase transition with Wilson fermions at zero and imaginary chemical potential. Phys. Rev. D **93**, 114507 (2016). doi:10.1103/PhysRevD.93.114507

[15] Z. Fodor, S. D. Katz, A New method to study lattice QCD at finite temperature and chemical potential. Phys. Lett. B **534**, 87 (2002). doi:10.1016/S0370-2693(02)01583-6

[16] K. Fukushima, C. Sasaki, The phase diagram of nuclear and quark matter at high baryon density. Prog. Part. Nucl. Phys. **72**, 99 (2013). doi:10.1016/j.ppnp.2013.05.003

[17] P. Braun-Munzinger, V. Koch, T. Schäfer et al., Properties of hot and dense matter from relativistic heavy ion collisions. Phys. Rept. **621**, 76 (2016). doi:10.1016/j.physrep.2015.12.003

[18] A. Bashir, L. Chang, I. C. Cloet et al., Collective perspective on advances in Dyson-Schwinger Equation QCD. Commun. Theor. Phys. **58**, 79-134 (2012). doi:10.1088/0253-6102/58/1/16

[19] C. S. Fischer, QCD at finite temperature and chemical potential from Dyson-Schwinger equations," Prog. Part. Nucl. Phys. **105**, 1-60 (2019). doi:10.1016/j.ppnp.2019.01.002

[20] B. J. Schaefer, J. Wambach, Renormalization group approach towards the QCD phase diagram. Phys. Part. Nucl. **39**, 1025-1032 (2008). doi:10.1134/S1063779608070083

[21] H. Gies, Introduction to the functional RG and applications to gauge theories. Lect. Notes Phys. **852**, 287-348 (2012). doi:10.1007/978-3-642-27320-9_6

[22] Y. Nambu, G. Jona-Lasinio, Dynamical Model of Elementary Particles Based on an Analogy with Superconductivity. 1. Phys. Rev. **122**, 345-358 (1961). doi:10.1103/PhysRev.122.345

[23] Y. Nambu, G. Jona-Lasinio, Dynamical Model of Elementary Particles Based on an Analogy with Superconductivity. 2. Phys. Rev. **124**, 246-254 (1961). doi:10.1103/PhysRev.124.246

[24] C. Ratti, S. Roessner, M. A. Thaler et al., Thermodynamics of the PNJL model. Eur. Phys. J. C **49**, 213 (2007).

doi:10.1140/epjc/s10052-006-0065-x

[25] K. Fukushima, Phase diagrams in the three-flavor Nambu-Jona-Lasinio model with the Polyakov loop. Phys. Rev. D **77**, 114028 (2008). doi:10.1103/PhysRevD.77.114028

[26] B. J. Schaefer, J. Wambach, Susceptibilities near the QCD (tri)critical point. Phys. Rev. D **75**, 085015 (2007). doi:10.1103/PhysRevD.75.085015

[27] B. J. Schaefer, M. Wagner, The three-flavor chiral phase structure in hot and dense QCD matter. Phys. Rev. D **79**, 014018 (2009). doi:10.1103/PhysRevD.79.014018

[28] B. J. Schaefer, J. M. Pawlowski, J. Wambach, The Phase Structure of the Polyakov-Quark-Meson Model. Phys. Rev. D **76**, 074023 (2007). doi:10.1103/PhysRevD.76.074023

[29] B. J. Schaefer, M. Wagner, QCD critical region and higher moments for three flavor models. Phys. Rev. D **85**, 034027 (2012). doi:10.1103/PhysRevD.85.034027

[30] Z. Zhang, C. Shi, X. T. He et al., Chiral phase transition inside a rotating cylinder within the Nambu–Jona-Lasinio model. Phys. Rev. D **102**, 114023 (2020). doi:10.1103/PhysRevD.102.114023

[31] Y. Jiang, J. Liao, Pairing Phase Transitions of Matter under Rotation. Phys. Rev. Lett. **117**, 192302 (2016). doi:10.1103/PhysRevLett.117.192302

[32] R. Gatto, M. Ruggieri, Deconfinement and Chiral Symmetry Restoration in a Strong Magnetic Background. Phys. Rev. D **83**, 034016 (2011). doi:10.1103/PhysRevD.83.034016

[33] K. Kashiwa, Entanglement between chiral and deconfinement transitions under strong uniform magnetic background field. Phys. Rev. D **83**, 117901 (2011). doi:10.1103/PhysRevD.83.117901

[34] M. D'Elia, F. Manigrasso, F. Negro et al., QCD phase diagram in a magnetic background for different values of the pion mass. Phys. Rev. D **98**, 054509 (2018). doi:10.1103/PhysRevD.98.054509

[35] G. S. Bali, F. Bruckmann, G. Endrodi et al., The QCD phase diagram for external magnetic fields. JHEP **1202**, 044 (2012). doi:10.1007/JHEP02(2012)044

[36] Y. P. Zhao, R. R. Zhang, H. Zhang et al., Chiral phase transition from the Dyson-Schwinger equations in a finite spherical volume. Chin. Phys. C **43**, 063101 (2019). doi:10.1088/1674-1137/43/6/063101

[37] R. A. Tripolt, J. Braun, B. Klein et al., Effect of fluctuations on the QCD critical point in a finite volume. Phys. Rev. D **90**, 054012 (2014). doi:10.1103/PhysRevD.90.054012

[38] A. Bhattacharyya, P. Deb, S. K. Ghosh et al., Thermodynamic Properties of Strongly Interacting Matter in Finite Volume using Polyakov-Nambu-Jona-Lasinio Model. Phys. Rev. D **87**, 054009 (2013). doi:10.1103/PhysRevD.87.054009

[39] N. Magdy, Influence of Finite Volume Effect on the Polyakov Quark–Meson Model. Universe **5**, 94 (2019). doi:10.3390/universe5040094

[40] P. Deb, S. Ghosh, J. Prakash et al., Finite size effect on Dissociation and Diffusion of chiral partners in Nambu-Jona-Lasinio model. Chin. Phys. C **46**, 044102 (2022). doi:10.1088/1674-1137/ac3def

[41] Y. P. Zhao, S. Y. Zuo, C. M. Li, QCD chiral phase transition and critical exponents within the nonextensive Polyakov-Nambu-Jona-Lasinio model. Chin. Phys. C **45**, 073105 (2021). doi:10.1088/1674-1137/abf8a2

[42] K. M. Shen, H. Zhang, D. F. Hou et al., Chiral Phase Transition in Linear Sigma Model with Nonextensive Statistical Mechanics. Adv. High Energy Phys. **2017**, 4135329 (2017). doi:10.1155/2017/4135329

[43] W. R. Tavares, R. L. S. Farias, S. S. Avancini, Deconfinement and chiral phase transitions in quark matter with a strong electric field. Phys. Rev. D **101**, 016017 (2020). doi:10.1103/PhysRevD.101.016017

[44] M. Ruggieri, Z. Y. Lu, G. X. Peng, Influence of chiral chemical potential, parallel electric, and magnetic fields on the critical temperature of QCD. Phys. Rev. D **94**, 116003 (2016). doi:10.1103/PhysRevD.94.116003

[45] G. Cao, X. G. Huang, Chiral phase transition and Schwinger mechanism in a pure electric field. Phys. Rev. D **93**, 016007 (2016). doi:10.1103/PhysRevD.93.016007

[46] C. Shi, X. T. He, W. B. Jia et al., Chiral transition and the chiral charge density of the hot and dense QCD matter. JHEP **2006**, 122 (2020). doi:10.1007/JHEP06(2020)122

[47] Y. Lu, Z. F. Cui, Z. Pan et al., QCD phase diagram with a chiral chemical potential. Phys. Rev. D **93**, 074037 (2016). doi:10.1103/PhysRevD.93.074037

[48] L. Yu, H. Liu, M. Huang, Effect of the chiral chemical potential on the chiral phase transition in the NJL model with different regularization schemes. Phys. Rev. D **94**, 014026 (2016). doi:10.1103/PhysRevD.94.014026

[49] R. L. S. Farias, D. C. Duarte, G. Krein et al., Thermodynamics of quark matter with a chiral imbalance. Phys. Rev. D **94**, 074011 (2016). doi:10.1103/PhysRevD.94.074011

[50] C. Shen, L. Yan, Recent development of hydrodynamic modeling in heavy-ion collisions," Nucl. Sci. Tech. **31**, 122 (2020). doi:10.1007/s41365-020-00829-z

[51] S. Wu, C. Shen, H. Song, Dynamically Exploring the QCD Matter at Finite Temperatures and Densities: A Short Review. Chin. Phys. Lett. **38**, 081201 (2021). doi:10.1088/0256-307X/38/8/081201

[52] J. F. Xu, Bulk viscosity of interacting magnetized strange quark matter. Nucl. Sci. Tech. **32**, 111 (2021). doi:10.1007/s41365-021-00954-3

[53] P. Romatschke, U. Romatschke, Viscosity Information from Relativistic Nuclear Collisions: How Perfect is the Fluid Observed at RHIC?. Phys. Rev. Lett. **99**, 172301 (2007). doi:10.1103/PhysRevLett.99.172301

[54] R. Marty, E. Bratkovskaya, W. Cassing et al., Transport coefficients from the Nambu-Jona-Lasinio model for $SU(3)_f$. Phys. Rev. C **88**, 045204 (2013). doi:10.1103/PhysRevC.88.045204

[55] S. Ghosh, T. C. Peixoto, V. Roy et al., Shear and bulk viscosities of quark matter from quark-meson fluctuations in the Nambu–Jona-Lasinio model. Phys. Rev. C **93**, 045205 (2016). doi:10.1103/PhysRevC.93.045205

[56] S. K. Ghosh, S. Raha, R. Ray et al., Shear viscosity and phase diagram from Polyakov–Nambu–Jona-Lasinio model. Phys. Rev. D **91**, 054005 (2015). doi:10.1103/PhysRevD.91.054005

[57] P. Zhuang, J. Hufner, S. P. Klevansky et al., Transport properties of a quark plasma and critical scattering at the chiral phase transition. Phys. Rev. D **51**, 3728 (1995). doi:10.1103/PhysRevD.51.3728

[58] P. Rehberg, S. P. Klevansky, J. Hufner, Elastic scattering and transport coefficients for a quark plasma in SU-f(3) at finite temperatures. Nucl. Phys. A **608**, 356-388 (1996). doi:10.1016/0375-9474(96)00247-3

[59] V. Mykhaylova, M. Bluhm, K. Redlich et al., Quark-flavor dependence of the shear viscosity in a quasiparticle model. Phys. Rev. D **100**, 034002 (2019). doi:10.1103/PhysRevD.100.034002

[60] O. Soloveva, P. Moreau, E. Bratkovskaya, Transport coefficients for the hot quark-gluon plasma at finite chem-

ical potential μ_B. Phys. Rev. C **101**, 045203 (2020). doi:10.1103/PhysRevC.101.045203

[61] H. B. Meyer, A Calculation of the shear viscosity in SU(3) gluodynamics. Phys. Rev. D **76**, 101701 (2007). doi:10.1103/PhysRevD.76.101701

[62] L. McLerran, V. Skokov, Comments About the Electromagnetic Field in Heavy-Ion Collisions. Nucl. Phys. A **929**, 184 (2014). doi:10.1016/j.nuclphysa.2014.05.008

[63] S. Gupta, The Electrical conductivity and soft photon emissivity of the QCD plasma. Phys. Lett. B **597**, 57 (2004). doi:10.1016/j.physletb.2004.05.079

[64] Y. Yin, Electrical conductivity of the quark-gluon plasma and soft photon spectrum in heavy-ion collisions. Phys. Rev. C **90**, 044903 (2014). doi:10.1103/PhysRevC.90.044903

[65] J. Hammelmann, J. M. Torres-Rincon, J. B. Rose et al., Electrical conductivity and relaxation via colored noise in a hadronic gas. Phys. Rev. D **99**, 076015 (2019). doi:10.1103/PhysRevD.99.076015

[66] W. Cassing, O. Linnyk, T. Steinert et al., Electrical Conductivity of Hot QCD Matter. Phys. Rev. Lett. **110**, 182301 (2013). doi:10.1103/PhysRevLett.110.182301

[67] M. Greif, I. Bouras, C. Greiner et al., Electric conductivity of the quark-gluon plasma investigated using a perturbative QCD based parton cascade. Phys. Rev. D **90**, 094014 (2014). doi:10.1103/PhysRevD.90.094014

[68] G. Aarts, A. Nikolaev, Electrical conductivity of the quark-gluon plasma: perspective from lattice QCD. Eur. Phys. J. A **57**, 118 (2021). doi:10.1140/epja/s10050-021-00436-5

[69] A. Amato, G. Aarts, C. Allton et al., Electrical conductivity of the quark-gluon plasma across the deconfinement transition. Phys. Rev. Lett. **111**, 172001 (2013). doi:10.1103/PhysRevLett.111.172001

[70] A. Das, H. Mishra, R. K. Mohapatra, Transport coefficients of hot and dense hadron gas in a magnetic field: a relaxation time approach. Phys. Rev. D **100**, 114004 (2019). doi:10.1103/PhysRevD.100.114004

[71] G. P. Kadam, H. Mishra, L. Thakur, Electrical and thermal conductivities of hot and dense hadronic matter. Phys. Rev. D **98**, 114001 (2018). doi:10.1103/PhysRevD.98.114001

[72] V. Mykhaylova, C. Sasaki, Impact of quark quasiparticles on transport coefficients in hot QCD. Phys. Rev. D **103**, 014007 (2021). doi:10.1103/PhysRevD.103.014007

[73] P. K. Srivastava, L. Thakur, B. K. Patra, Electrical Conductivity of an Anisotropic Quark Gluon Plasma : A Quasiparticle Approach. Phys. Rev. C **91**, 044903 (2015). doi:10.1103/PhysRevC.91.044903

[74] O. Soloveva, D. Fuseau, J. Aichelin et al., Shear viscosity and electric conductivity of a hot and dense QGP with a chiral phase transition. Phys. Rev. C **103**, 054901 (2021). doi:10.1103/PhysRevC.103.054901

[75] P. Sahoo, S. K. Tiwari, R. Sahoo, Electrical conductivity of hot and dense QCD matter created in heavy-ion collisions: A color string percolation approach. Phys. Rev. D **98**, 054005 (2018). doi:10.1103/PhysRevD.98.054005

[76] S. Jain, Universal thermal and electrical conductivity from holography. JHEP **1011**, 092 (2010). doi:10.1007/JHEP11(2010)092

[77] L. Thakur, P. K. Srivastava, Electrical conductivity of a hot and dense QGP medium in a magnetic field. Phys. Rev. D **100**, 076016 (2019). doi:10.1103/PhysRevD.100.076016

[78] M. Kurian, V. Chandra, Effective description of hot QCD medium in strong magnetic field and longitudinal conductivity. Phys. Rev. D **96**, 114026 (2017).

doi:10.1103/PhysRevD.96.114026

[79] S. Rath, B. K. Patra, Effect of magnetic field on the charge and thermal transport properties of hot and dense QCD matter. Eur. Phys. J. C **80**, 747 (2020). doi:10.1140/epjc/s10052-020-8331-x

[80] A. Das, H. Mishra, R. K. Mohapatra, Magneto-Seebeck coefficient and Nernst coefficient of a hot and dense hadron gas. Phys. Rev. D **102**, 014030 (2020). doi:10.1103/PhysRevD.102.014030

[81] J. R. Bhatt, A. Das, H. Mishra, Thermoelectric effect and Seebeck coefficient for hot and dense hadronic matter. Phys. Rev. D **99**, 014015 (2019). doi:10.1103/PhysRevD.99.014015

[82] H. X. Zhang, J. W. Kang, B. W. Zhang, Thermoelectric properties of the (an-)isotropic QGP in magnetic fields. Eur. Phys. J. C **81**, 623 (2021). doi:10.1140/epjc/s10052-021-09409-w

[83] D. Dey, B. K. Patra, Seebeck effect in a thermal QCD medium in the presence of strong magnetic field. Phys. Rev. D **102**, 096011 (2020). doi:10.1103/PhysRevD.102.096011

[84] A. Abhishek, A. Das, D. Kumar et al., Thermoelectric transport coefficients of quark matter. Eur. Phys. J. C **82**, 71 (2022). doi:10.1140/epjc/s10052-022-09999-z

[85] M. Strickland, Anisotropic Hydrodynamics: Three lectures. Acta Phys. Polon. B **45**, 2355-2394 (2014). doi:10.5506/APhysPolB.45.2355

[86] P. Romatschke, M. Strickland, Collective modes of an anisotropic quark gluon plasma. Phys. Rev. D **68**, 036004 (2003). doi:10.1103/PhysRevD.68.036004

[87] B. S. Kasmaei, M. Strickland, Photon production and elliptic flow from a momentum-anisotropic quark-gluon plasma. Phys. Rev. D **102**, 014037 (2020). doi:10.1103/PhysRevD.102.014037

[88] B. Schenke, M. Strickland, Photon production from an anisotropic quark-gluon plasma. Phys. Rev. D **76**, 025023 (2007). doi:10.1103/PhysRevD.76.025023

[89] B. S. Kasmaei, M. Strickland, Parton self-energies for general momentum-space anisotropy. Phys. Rev. D **97**, 054022 (2018). doi:10.1103/PhysRevD.97.054022

[90] R. Ghosh, B. Karmakar, A. Mukherjee, Covariant formulation of gluon self-energy in presence of ellipsoidal anisotropy. Phys. Rev. D **102**, 114002 (2020). doi:10.1103/PhysRevD.102.114002

[91] A. Dumitru, Y. Guo, M. Strickland, The Heavy-quark potential in an anisotropic (viscous) plasma. Phys. Lett. B **662**, 37 (2008). doi:10.1016/j.physletb.2008.02.048

[92] L. Thakur, P. K. Srivastava, G. P. Kadam et al., Shear viscosity η to electrical conductivity σ_{el} ratio for an anisotropic QGP. Phys. Rev. D **95**, 096009 (2017). doi:10.1103/PhysRevD.95.096009

[93] S. Rath, B. K. Patra, Revisit to electrical and thermal conductivities, Lorenz and Knudsen numbers in thermal QCD in a strong magnetic field. Phys. Rev. D **100**, 016009 (2019). doi:10.1103/PhysRevD.100.016009

[94] R. Baier, Y. Mehtar-Tani, Jet quenching and broadening: The Transport coefficient q-hat in an anisotropic plasma. Phys. Rev. C **78**, 064906 (2008). doi:10.1103/PhysRevC.78.064906

[95] M. Alqahtani, M. Nopoush, M. Strickland, Relativistic anisotropic hydrodynamics. Prog. Part. Nucl. Phys. **101**, 204 (2018). doi:10.1016/j.ppnp.2018.05.004

[96] W. M. Zhang, L. Wilets, Transport theory of relativistic heavy ion collisions with chiral symmetry. Phys. Rev. C **45**, 1900-1917 (1992). doi:10.1103/PhysRevC.45.1900

[97] W. Botermans, R. Malfliet, Quantum transport theory of nuclear matter. Phys. Rept. **198**, 115-194 (1990).

doi:10.1016/0370-1573(90)90174-Z

[98] P. Rehberg, Relativistic transport theory for systems containing bound states. Phys. Rev. C **57**, 3299-3313 (1998). doi:10.1103/PhysRevC.57.3299

[99] P. Rehberg, J. Hufner, A Numerical study of an expanding plasma of quarks in a chiral model. Nucl. Phys. A **635**, 511-541 (1998). doi:10.1016/S0375-9474(98)00184-5

[100] S. P. Klevansky, A. Ogura, J. Hufner, Derivation of transport equations for a strongly interacting Lagrangian in powers of anti-H and 1 / N(c). Annals Phys. **261**, 37-73 (1997). doi:10.1006/aphy.1997.5734

[101] S. P. Klevansky, Chiral symmetry breaking in hot matter. Lect. Notes Phys. **516**, 113-161 (1999). doi:10.1007/BFb0107313

[102] Z. Wang, S. Shi, P. Zhuang, Chiral Phase Transition in an Expanding Quark System. Phys. Rev. C **103**, 014901 (2021). doi:10.1103/PhysRevC.103.014901

[103] P. Rehberg, S. P. Klevansky, J. Hufner, Hadronization in the SU(3) Nambu-Jona-Lasinio model. Phys. Rev. C **53**, 410 (1996). doi:10.1103/PhysRevC.53.410

[104] P. Rehberg, Y. L. Kalinovsky, D. Blaschke, Critical scattering and two photon spectra for a quark / meson plasma. Nucl. Phys. A **622**, 478 (1997). doi:10.1016/S0375-9474(97)82592-4

[105] P. Rehberg, S. P. Klevansky, One loop integrals at finite temperature and density. Annals Phys. **252**, 422 (1996). doi:10.1006/aphy.1996.0140

[106] A. L. Fetter, J. D. Walecka, *Quantum Theory of Many Particle Systems* (McGraw-Hill Book Co, New York, 1971).

[107] A. Dumitru, Y. Guo, M. Strickland, The Imaginary part of the static gluon propagator in an anisotropic (viscous) QCD plasma. Phys. Rev. D **79**, 114003 (2009). doi:10.1103/PhysRevD.79.114003

[108] P. Romatschke, Momentum broadening in an anisotropic plasma. Phys. Rev. C **75**, 014901 (2007). doi:10.1103/PhysRevC.75.014901

[109] M. Asakawa, S. A. Bass, B. Muller, Anomalous transport processes in anisotropically expanding quark-gluon plasmas. Prog. Theor. Phys. **116**, 725 (2007). doi:10.1143/PTP.116.725

[110] A. Dumitru, Y. Guo, A. Mocsy et al., Quarkonium states in an anisotropic QCD plasma. Phys. Rev. D **79**, 054019 (2009). doi:10.1103/PhysRevD.79.054019

[111] A. Hosoya, K. Kajantie, Transport Coefficients of QCD Matter. Nucl. Phys. B **250**, 666 (1985). doi:10.1016/0550-3213(85)90499-7

[112] L.D. Landau, E.M. Lifshitz, *Fluid Mechanics* (Butterworth-Heinemann, Oxford, 1987).

[113] A. Jaiswal, B. Friman, K. Redlich, Relativistic second-order dissipative hydrodynamics at finite chemical potential. Phys. Lett. B **751**, 548 (2015). doi:10.1016/j.physletb.2015.11.018

[114] D. M. Rowe, *Thermoelectrics and its Energy Harvesting* Vol 1 (CRC Press, Boca Raton, 2012).

[115] H. J. Goldsmid, *Thermoelectric Refrigeration*, (Plenum Press,s New York, 1964).

[116] P. Danielewicz, M. Gyulassy, Dissipative Phenomena in Quark Gluon Plasmas. Phys. Rev. D **31**, 53 (1985). doi:10.1103/PhysRevD.31.53

[117] M. Buballa, NJL model analysis of quark matter at large density. Phys. Rept. **407**, 205-376 (2005). doi:10.1016/j.physrep.2004.11.004

[118] N. Chaudhuri, S. Ghosh, S. Sarkar et al., Effect of the anomalous magnetic moment of quarks on the phase structure and mesonic properties in the NJL model. Phys. Rev. D **99**, 116025 (2019). doi:10.1103/PhysRevD.99.116025

[119] M. Martinez, M. Strickland, Pre-equilibrium dilepton production from an anisotropic quark-gluon plasma. Phys. Rev. C **78**, 034917 (2008). doi:10.1103/PhysRevC.78.034917

[120] A. V. Friesen, Y. V. Kalinovsky, V. D. Toneev, Quark scattering off quarks and hadrons. Nucl. Phys. A **923**, 1 (2014). doi:10.1016/j.nuclphysa.2014.01.002